Chapter 2
Excitation and Propagation of SLF/ELF Electromagnetic Waves in the Earth–Ionosphere Waveguide/Cavity

In this chapter, the region of interest is a waveguide or cavity between the Earth's surface and an isotropic homogeneous ionosphere. The dipole (vertical electric dipole (VED), the vertical magnetic dipole (VMD), or the horizontal electric dipole (HED)) and the observation point are assumed to be located on or near the spherical surface of the Earth. The approximate all formulas are obtained for the electromagnetic field radiated by a VED and a VMD in the Earth–ionosphere waveguide or cavity. Based on the above results, the approximate formulas are derived readily for the electromagnetic field of an HED in the Earth–ionosphere waveguide or cavity by using the reciprocity theorem. Analyses and computations in SLF/ELF ranges are carried out specifically.

2.1 Introduction

The properties of the electromagnetic field generated by a VLF/ULF/SLF/ELF dipole source in the Earth–ionosphere waveguide or cavity have been investigated widely in the past 60 years because of its useful applications in submarine communication, navigation, geophysical prospecting and diagnostics, and earthquake electromagnetic detection (Bouwkamp and Casimir 1954; Budden 1961; Wait 1970; Galejs 1972a; Felsen and Marcuvitz 1973; Nickolaenko and Hayakawa 2002).

Remarkable progresses in VLF electromagnetic wave propagation in the Earth–ionosphere waveguide were made by many researchers, especially including several pioneers such as Budden (1961), Wait (1957, 1960, 1970), Wait and Spies (1965), and Galejs (1964, 1968, 1970, 1972a, 1972b). In early works by Wait and Galejs, the problem on VLF wave propagation in an Earth–ionosphere waveguide was treated analytically. In 1992, Wait examined analytically the problem on VLF radio wave propagation in an inhomogeneous Earth–ionosphere waveguide Wait (1992). Obviously, those works in VLF ranges were extended in the study on SLF/ELF radio wave propagation in the Earth–ionosphere waveguide or cavity (Wait 1957,

W. Pan, K. Li, *Propagation of SLF/ELF Electromagnetic Waves*,
Advanced Topics in Science and Technology in China,
DOI 10.1007/978-3-642-39050-0_2,

1960, 1970; Wait and Spies 1965; and Suchumann 1952a, 1952b; Galejs 1964, 1972a, 1972b). Based on the pioneering works by Budden, Wait, and Galejs, further works were also carried out by many researchers (Bannister et al. 1973; Bannister 1984; Tripathi et al. 1982; Carroll and Ferraro 1990; Fraser-Smith and Bannister 1998; Cummer 2000; Wang et al. 2005, 2008). In recent years, SLF/ELF wave propagation in the anisotropic Earth–ionosphere waveguide or cavity are treated analytically (Rybachek and Ponomariev 2007; Kirillov and Pronin 2007; Li 2012).

In the 1970s, some works in SLF/ELF wave propagation in the Earth–ionosphere waveguide or cavity were also carried out by Pan in China and summarized in a recent book (Pan 2004). In what follows, we will summarize some works on SLF/ELF wave propagation by Pan in the 1970s and some new research results in our research groups. In this chapter, the region of interest is a space between an electrically homogeneous Earth and a homogeneous ionosphere and both the dipole source and the observation point are assumed on or near the Earth's surface. First, the approximate formulas are obtained for the electromagnetic field of VEDs and VMDs in the Earth–ionosphere waveguide or cavity. Based on the results obtained, the approximate formulas are derived readily for the electromagnetic field of an HED in the Earth–ionosphere waveguide or cavity by using the reciprocity theorem. Finally, computations and analyses are carried out in SLF/ELF frequency ranges.

2.2 SLF/ELF Field of VED in the Earth–Ionosphere Waveguide/Cavity

In this section, we will summarize the derivations and analyses on the electromagnetic field of a VED in the Earth–ionosphere waveguide or cavity, which were carried out by Pan in the 1970s (Pan 2004). The results by Pan, in which the derivations are different from the available results, are similar to those by Galejs (1972a).

2.2.1 Formulations of the Problem

In SLF/ELF ranges, the effective waveguide height h, which is only 60–90 km, is less than the free-space wavelength λ, and only a zero-order mode can propagate. The geometry under consideration is the same as Fig. 2.1 in Chap. 1. We assume that a VED is represented by its current density, $\widehat{z}I\,\mathrm{d}l\delta(x)\delta(y)\delta(z-b)$, where $b = z_s + a$, and $z_s > 0$ denotes the height of the dipole above the Earth's surface. The field components, for the TM waves radiated by a VED, are expressed as follows:

$$E_r = \left(\frac{\partial^2}{\partial r^2} + k^2\right)(Ur), \tag{2.1}$$

$$E_\theta = \frac{1}{r}\frac{\partial^2}{\partial\theta\partial r}(Ur), \tag{2.2}$$

$$H_\phi = \frac{\mathrm{i}\omega\varepsilon}{r}\frac{\partial}{\partial\theta}(Ur), \tag{2.3}$$

$$H_r = H_\theta = E_\phi = 0. \tag{2.4}$$

Here the potential functions U satisfy the scalar Helmholtz equation,

$$\left(\nabla^2 + k^2\right)U = 0. \tag{2.5}$$

It is noted that the normalized surface impedances at the boundaries can be represented as follows:

$$\left.\frac{E_\theta}{\eta_1 H_\phi}\right|_{r=a} = -\Delta_g; \qquad \left.\frac{E_\theta}{\eta_1 H_\phi}\right|_{r=a+h} = \Delta_i, \tag{2.6}$$

where η_1 is the wave impedance of the air, and Δ_g and Δ_i are the normalized Earth's surface impedance and the normalized ionospheric surface impedance, respectively.

With the substitution of Eqs. (2.2) and (2.3) into Eq. (2.6), the boundary conditions are written as follows:

$$\left.\frac{1}{rU}\frac{\mathrm{d}}{\mathrm{d}r}(rU)\right|_{r=a} = -\mathrm{i}k\Delta_g, \tag{2.7}$$

$$\left.\frac{1}{rU}\frac{\mathrm{d}}{\mathrm{d}r}(rU)\right|_{r=a+h} = \mathrm{i}k\Delta_i. \tag{2.8}$$

In a spherical coordinate system, because of symmetry, the expanded form of Eq. (2.5) can be written as follows:

$$\frac{1}{r^2}\frac{\partial}{\partial r}\left(r^2\frac{U}{r}\right) + \frac{1}{r^2\sin\theta}\frac{\partial}{\partial\theta}\left(\sin\theta\frac{\partial U}{\partial\theta}\right) + k^2U = 0. \tag{2.9}$$

The solution of the potential function U is represented in the form

$$U = \frac{1}{r}F(r)\Phi(\theta). \tag{2.10}$$

Then, we have

$$\frac{1}{\sin\theta}\frac{\mathrm{d}}{\mathrm{d}\theta}\left[\sin\theta\frac{\mathrm{d}\Phi(\theta)}{\mathrm{d}\theta}\right] + \nu(\nu+1)\Phi(\theta) = 0, \tag{2.11}$$

$$\frac{\mathrm{d}^2F(r)}{\mathrm{d}r^2} + k^2\left[1 - \frac{\nu(\nu+1)}{k^2r^2}\right]F(r) = 0. \tag{2.12}$$

With the substitutions of $x = \cos(\pi - \theta)$ and $\theta = \pi - \arccos x$, Eq. (2.11) can be transformed into the standard Legendre equation. We write

$$\left(1 - x^2\right)\frac{\mathrm{d}^2\Phi}{\mathrm{d}x^2} - 2x\frac{\mathrm{d}\Phi}{\mathrm{d}x} + \nu(\nu+1)\Phi = 0. \tag{2.13}$$

The two solutions of Eq. (2.13) can be expressed by $P_\nu(\cos(\pi - \theta))$ and $Q_\nu(\cos(\pi - \theta))$, respectively. It is seen that the Legendre function of the first kind $P_\nu(\cos(\pi - \theta))$ has only one pole in the situation of the dipole source with $x = -1$ or $\theta = 0$. The Legendre function of the second kind has two poles at $x = \pm 1$. Obviously, the Legendre function of the second kind $Q_\nu(\cos(\pi - \theta))$ should not be included in the solutions of Eq. (2.11). We take

$$\Phi(\theta) = P_\nu\big(\cos(\pi - \theta)\big). \tag{2.14}$$

In the space between the Earth's surface and the lower boundary of the ionosphere, we have $a \le r \le a + h$, and h is very small compared with a. That is to say, $1 - \frac{\nu(\nu+1)}{k^2r^2}$ changes very slowly in the region of $a \le r \le a + h$. Thus the WKB approximation can be taken in this case, and the two solutions of Eq. (2.12) can be obtained readily. We have

$$F_1(r) = \frac{1}{4\sqrt{1 - \frac{\nu(\nu+1)}{k^2r^2}}}\exp\left(\mathrm{i}k\int_a^r\left[1 - \frac{\nu(\nu+1)}{k^2t^2}\right]^{\frac{1}{2}}\mathrm{d}t\right), \tag{2.15}$$

and

$$F_2(r) = \frac{1}{4\sqrt{1 - \frac{\nu(\nu+1)}{k^2r^2}}}\exp\left(-\mathrm{i}k\int_a^r\left[1 - \frac{\nu(\nu+1)}{k^2t^2}\right]^{\frac{1}{2}}\mathrm{d}t\right), \tag{2.16}$$

where the first solution represents the wave propagating in the direction when r increases, while the second solution represents the wave propagating in the direction of decreasing r.

Letting $r = a + z_r$, $z_r > 0$ denotes the height of the observation point above the Earth's surface. It is assumed that both the dipole and the observation point are on or close to the Earth's surface. Obviously, we have $z_s \ll a$ and $z_r \ll a$. Then, the following approximation can be taken as:

$$\frac{\nu(\nu+1)}{k_0^2r^2} \approx \frac{\nu(\nu+1)}{k_0^2a^2}\left(1 - \frac{2z_r}{a}\right). \tag{2.17}$$

Thus, the solution of Eq. (2.12) in the Earth–ionosphere cavity becomes

$$\begin{aligned} F(z_r) = {} & A\exp\left[-\mathrm{i}k\int_a^r\left(C^2 + \frac{2z}{a}S^2\right)^{\frac{1}{2}}\mathrm{d}t\right] \\ & + B\exp\left[\mathrm{i}k\int_a^r\left(C^2 + \frac{2z}{a}S^2\right)^{\frac{1}{2}}\mathrm{d}t\right], \end{aligned} \tag{2.18}$$

where the parameters C and S are defined by

$$S^2 = \frac{\nu(\nu+1)}{k^2 a^2}; \qquad C^2 = 1 - S^2. \tag{2.19}$$

From Eqs. (2.7) and (2.8), the boundary conditions are rewritten as follows:

$$\left[\frac{1}{F(z)}\frac{\mathrm{d}}{\mathrm{d}z}F(z)\right]\Big|_{z=0} = -\mathrm{i}k\Delta_g, \tag{2.20}$$

$$\left[\frac{1}{F(z)}\frac{\mathrm{d}}{\mathrm{d}z}F(z)\right]\Big|_{z=h} = \mathrm{i}k\Delta_i. \tag{2.21}$$

With Eq. (2.20), the reflection coefficient R_g of the lower boundary (Earth–air boundary) can be obtained readily. It is

$$R_g = \frac{B}{A} = \frac{C-\Delta_g}{C+\Delta_g}. \tag{2.22}$$

Applying Eq. (2.18) into Eq. (2.21), we get

$$\begin{aligned}&\left\{1 - R_g \exp\left[2\mathrm{i}k\int_0^h \left(C^2 + \frac{2z}{a}S^2\right)^{\frac{1}{2}}\mathrm{d}z\right]\right\}\cdot\left(C^2 + \frac{2h}{a}S^2\right)\\ &\quad = -\Delta_i\left\{1 + R_g \exp\left[2\mathrm{i}k\int_0^h \left(C^2 + \frac{2z}{a}S^2\right)^{\frac{1}{2}}\mathrm{d}z\right]\right\}.\end{aligned} \tag{2.23}$$

It is noted that

$$C' = \left(C^2 + \frac{2h}{a}S^2\right)^{\frac{1}{2}}; \qquad R_i = \frac{C'-\Delta_i}{C'+\Delta_i}, \tag{2.24}$$

where R_i is the reflection coefficient of the upper boundary (air–ionosphere boundary). Then, the modal equation can be obtained readily. We write

$$R_g R_i \exp\left[2\mathrm{i}k\int_0^h \left(C^2 + \frac{2z}{a}S^2\right)^{\frac{1}{2}}\mathrm{d}z\right] = 1. \tag{2.25}$$

If C_n is the nth root, the normalized height-gain function $F_n(z)$ is expressed in the following form:

$$\begin{aligned}F_n(z_r) = \frac{1}{1+R_g}\Bigg[&\exp\left(-\mathrm{i}k\int_0^{z_r}\sqrt{C_n^2 + \frac{2z}{a}S_n^2}\,\mathrm{d}z\right)\\ &+ R_g \exp\left(\mathrm{i}k\int_0^{z_r}\sqrt{C_n^2 + \frac{2z}{a}S_n^2}\,\mathrm{d}z\right)\Bigg].\end{aligned} \tag{2.26}$$

From Eq. (2.19), we obtain

$$\nu(\nu+1) = k^2a^2S_n^2 = k^2a^2\left(1-C_n^2\right). \tag{2.27}$$

In practical wave modes in the Earth–ionosphere waveguide or cavity, the parameter C_n is not close to 1. Considering that the Earth's radius is very large, in SLF range, $k^2a^2 \gg 1$, it is seen that the parameter $|\nu|$ is a large number. Then, we write

$$\nu = kaS_n - \frac{1}{2}. \tag{2.28}$$

When the parameter $|\nu|$ is very large, namely $|\nu| \gg 1$, while the angle θ is not close to 0 and π, the Legendre function of the first kind is approximated by

$$\begin{aligned} P_\nu\left(\cos(\pi-\theta)\right) &\approx \left(\frac{2}{\pi\nu\sin\theta}\right)^{\frac{1}{2}} \cos\left[\left(\nu+\frac{1}{2}\right)(\pi-\theta)-\frac{\pi}{4}\right] \\ &= \left(\frac{1}{2\pi\nu\sin\theta}\right)^{\frac{1}{2}} \mathrm{e}^{-\mathrm{i}kaS_n\pi+\frac{\mathrm{i}\pi}{4}} \cdot \left[\mathrm{e}^{\mathrm{i}kaS_n\theta} + \mathrm{e}^{\mathrm{i}kaS_n(2\pi-\theta)-\frac{\mathrm{i}\pi}{2}}\right]. \end{aligned} \tag{2.29}$$

It is noted that the asymptotic form in Eq. (2.29) is not valid in the vicinity of the source ($\theta \to 0$) or in the vicinity of the antipole ($\theta \to \pi$). From Eq. (2.29), the function $P_\nu(\cos(\pi-\theta))$, which varies with the angle θ, includes the wave $\mathrm{e}^{\mathrm{i}kaS_n\theta}$ propagating along the short circular propagation path and the wave $\mathrm{e}^{\mathrm{i}kaS_n(2\pi-\theta)-\frac{\mathrm{i}\pi}{2}}$ propagating along the long circular propagation path, which travels over the antipole. It is seen that when the observation point is not close to the antipole, the wave propagating along the long circular propagation path can be neglected. Thus, we write

$$P_\nu\left(\cos(\pi-\theta)\right) \approx \left(\frac{1}{2\pi\nu\sin\theta}\right)^{\frac{1}{2}} \mathrm{e}^{-\mathrm{i}kaS_n\pi+\frac{\mathrm{i}\pi}{4}} \mathrm{e}^{\mathrm{i}kaS_n\theta}. \tag{2.30}$$

Then, we get

$$\begin{aligned} P_\nu\left(\cos(\pi-\theta)\right)F_n(z) \propto{}& \left(\frac{1}{\sin\theta}\right)^{\frac{1}{2}} \mathrm{e}^{\mathrm{i}kaS_n\theta} \\ &\times \left\{\exp\left[-\mathrm{i}k\int_0^z \left(C_n^2+\frac{2t}{a}S_n^2\right)^{\frac{1}{2}}\mathrm{d}t\right]\right. \\ &\left. + R_g\exp\left[\mathrm{i}k\int_0^z \left(C_n^2+\frac{2t}{a}S_n^2\right)^{\frac{1}{2}}\mathrm{d}t\right]\right\}. \end{aligned} \tag{2.31}$$

Obviously, each propagation mode includes the wave traveling to the Earth's surface with the angle $\theta_n = \arccos C_n$ and the corresponding reflected wave. It is noted that the phase velocity υ_n is inversely proportional to the real part of S_n, and

the attenuation rate is proportional to the imaginary part of S_n. Then, we write

$$\frac{\upsilon_n}{\mathrm{c}} = \frac{1}{\mathrm{Re}\, S_n} \approx \mathrm{Re}\left(1 + \frac{C_n^2}{2}\right), \tag{2.32}$$

$$\alpha_n = 8.68 \times \frac{2\pi\ \mathrm{Im} S_n}{\lambda} \approx 8.68 \times \frac{2\pi\ \mathrm{Im}(-\frac{C_n^2}{2})}{\lambda}\ (\mathrm{dB/km}). \tag{2.33}$$

In SLF/ELF ranges, both Δ_i and Δ_g are very small. Thus, the reflection coefficients R_i and R_g are approximated by

$$R_i \approx \exp\left(-2\Delta_i / C_n\right), \tag{2.34}$$

$$R_g \approx \exp(-2\Delta_g / C_n). \tag{2.35}$$

The approximated solutions of the mode equation (2.25) can be obtained readily. We write

$$C_n = \frac{n\pi}{2kh} + \sqrt{\left(\frac{n\pi}{2kh}\right)^2 - \frac{\mathrm{i}(\Delta_g + \Delta_i)}{kh}}, \tag{2.36}$$

$$S_n = \left\{1 - \left(\frac{n\pi}{2kh}\right)^2 \left(1 + \sqrt{1 - \frac{4\mathrm{i}(\Delta_g + \Delta_i)kh}{(n\pi)^2}}\right)\right\}^{1/2}. \tag{2.37}$$

For both Δ_i and Δ_g being very small, when $n\pi > 2kh$, the parameter S_n is a pure imaginary number, which represents an evanescent mode. For a typical daytime model with the ionospheric height $h = 70$ km, when $\lambda > 2h = 140$ km, $f < 2.2$ kHz, only the TM wave of zero order can propagate and the rest of the waves are evanescent. Similarly, for a typical nighttime model with the ionospheric height $h = 90$ km, when $\lambda > 2h = 180$ km, $f < 1.7$ kHz, only a zero-order TM mode can propagate and the rest, the high-order modes, are evanescent. Then, we have

$$C_0 \approx \mathrm{e}^{-\mathrm{i}\pi/4} \sqrt{\frac{\Delta_g + \Delta_i}{kh}}, \tag{2.38}$$

$$S_0 \approx \left[1 + \frac{\mathrm{i}(\Delta_g + \Delta_i)}{kh}\right]^{1/2}. \tag{2.39}$$

We examine the height-gain function $F_\mu(z)$, which is the solution of Eq. (2.12). At the Earth's surface $z = 0$, we have

$$F_\mu(0) = 1; \qquad F'_\mu(0) = -\mathrm{i}k\Delta_g. \tag{2.40}$$

It is noted that, for the parameter μ, its variations are regarded to be continuous. Both the height-gain functions $F_n(z)$ and $F_\mu(z)$ satisfy Eq. (2.12) and the boundary conditions at the Earth's surface. Then, we write

$$\int_0^h F_n(z) F_\mu(z) \mathrm{d}z = \frac{1}{k^2(S_n^2 - S_\mu^2)} \left[F_\mu(z) F'_n(z) - F_n(z) F'_\mu(z)\right]\Big|_0^h, \tag{2.41}$$

where

$$S_n^2 = \frac{\nu(\nu+1)}{k^2a^2}; \qquad S_\mu^2 = \frac{\mu(\mu+1)}{k^2a^2}. \tag{2.42}$$

Evidently, when $S_\mu \to S_n$, we have $F_\mu(z) \to F_n(z)$. Thus, we write

$$\begin{aligned} N_n &= \int_0^h F_n(z)F_n(z)\,\mathrm{d}z = \lim_{s_\mu \to s_n} \int_0^h F_n(z)F_\mu(z)\,\mathrm{d}z \\ &= \lim_{s_\mu \to s_n} \frac{1}{k(S_n^2 - S_\mu^2)}\left[F_n'(h)F_\mu(h) - F_n(h)F_\mu'(h)\right] \\ &= \frac{1}{2k^2S_n}\left[F_n(h)\frac{\mathrm{d}F_n'(h)}{\mathrm{d}S_n} - F_n'(h)\frac{\mathrm{d}F_n(h)}{\mathrm{d}S_n}\right]. \end{aligned} \tag{2.43}$$

Letting

$$H = \int_0^h \left(C_n^2 + \frac{2z}{a}S_n^2\right)^{\frac{1}{2}}\mathrm{d}z = \frac{a}{3S_n^2}\left(C_n'^3 - C_n^3\right), \tag{2.44}$$

we have

$$\begin{aligned} N_n = {} & \frac{4R_g}{(1+R_g)^2}\frac{aC_n'}{3S_n^4}\left\{C_n'^3 - C_n^3 + \frac{3S_n^2}{2}\left[C_n'\left(1-\frac{2h}{a}\right) - C_n\right]\right\} \\ & - \frac{\mathrm{i}C_n'\Delta_g}{2C_n^3k} + \frac{\mathrm{i}(1-\frac{2h}{a})(\mathrm{e}^{-2\mathrm{i}kH} - R_g^2\mathrm{e}^{2\mathrm{i}kH})}{2kC_n'(1+R_g)^2}. \end{aligned} \tag{2.45}$$

In the case of the Earth being a perfect conducting sphere, $\Delta_g \approx 0$, $R_g \approx 1$. We obtain

$$\begin{aligned} N_n \approx {} & \frac{aC_n'}{3S_n^4}\left\{C'^3_n - C_n^3 + \frac{3S_n^2}{2}\left[C'_n\left(1-\frac{2h}{a}\right) - C_n\right]\right\} \\ & + \left(1-\frac{2h}{a}\right)\frac{\sin 2kH}{4kC_n'}. \end{aligned} \tag{2.46}$$

When $C_n^2 \gg \frac{2h}{a}$, we have

$$C_n'^3 - C_n^3 + \frac{3S_n^2}{2}\left[C_n'\left(1-\frac{2h}{a}\right) - C_n\right] \approx \frac{3hS_n^4}{2aC_n}. \tag{2.47}$$

Then, a further simplification gives

$$N_n \approx \frac{h}{2}\left(1 + \frac{\sin 2kC_nh}{2kC_nh}\right). \tag{2.48}$$

By now, the potential function U for the electromagnetic field of a VED in the Earth–ionosphere waveguide or cavity can be represented in the following

form:

$$U = \frac{1}{r}\sum_s A_s F_s(z_r) P_\nu\big(\cos(\pi-\theta)\big). \tag{2.49}$$

In the next step, it is necessary to determine the excitation coefficients A_s ($s = 0, 1, 2, \ldots$) in Eq. (2.49).

2.2.2 Determination of the Excitation Coefficients A_s

In the region of $|z_r - z_s| \le \delta$, where δ is a finite small value, when $\theta \to 0$, the influences of the electromagnetic field by both the Earth and the ionosphere can be neglected.

By multiplying the function $rF_n(z)$ on both sides of Eq. (2.49), and integrating from 0 to h for z, we have

$$A_n N_n P_\nu\big(\cos(\pi-\theta)\big) = \int_0^h rU F_n(z)\,\mathrm{d}z. \tag{2.50}$$

Obviously, the excitation coefficient A_n can be obtained by using the source singularity. Close to the source, the integral is written in the form

$$\begin{aligned}\int_0^h rU F_n(z)\,\mathrm{d}z = &\int_0^{z_s-\delta} rF_n(z)U\,\mathrm{d}z + \int_{z_s-\delta}^{z_s+\delta} rF_n(z)U\,\mathrm{d}z \\ &+ \int_{z_s+\delta}^{h} rF_n(z)U\,\mathrm{d}z,\end{aligned} \tag{2.51}$$

where δ is very small. When the conditions $|z - z_s| \le \delta$ and $\theta \to 0$ are satisfied, the potential function U is approximated by

$$U \xrightarrow{\theta\to 0,\ |z-z_s|<\delta} U_0 = \frac{C_0 \mathrm{e}^{\mathrm{i}kR}}{r_0 R} \approx \frac{\mathrm{i}I\,\mathrm{d}l}{4\pi\omega\varepsilon_0 r_0 R}, \tag{2.52}$$

where

$$R = \big(r^2 + r_0^2 - 2rr_0\cos\theta\big)^{\frac{1}{2}}; \qquad C_0 = \frac{\mathrm{i}I\,\mathrm{d}l}{4\pi\omega\varepsilon_0}. \tag{2.53}$$

In the above formulas, $r_0 = a + z_s$ and $r = a + z_r$. In the intervals $(0, z_s - \delta)$ and $(z_s + \delta, h)$, both U and $F_n(z)$ are continuous functions, and the integration from 0 to $z_s - \delta$ and that from $z_s + \delta$ to h in Eq. (2.51) are finite. Thus, we get

$$\begin{aligned}\int_0^h rF_n(z)U\,\mathrm{d}z &= r_0 F_n(z_s)\int_{z_s-\delta}^{z_s+\delta} U_0\,\mathrm{d}z + O(1) \\ &= \frac{\mathrm{i}F_n(z_s)I\,\mathrm{d}l}{4\pi\omega\varepsilon_0}\int_{z_s-\delta}^{z_s+\delta}\frac{\mathrm{d}z}{R} + O(1).\end{aligned} \tag{2.54}$$

Close to the source, we have

$$\cos\theta \approx 1 - \frac{\theta^2}{2}; \qquad R \approx r_0\left[\theta^2 + \frac{(z-z_s)^2}{r^2}\right]^{\frac{1}{2}}. \tag{2.55}$$

Then, we obtain

$$\int_{z_s-\delta}^{z_s+\delta} \frac{\mathrm{d}z}{R} \approx \ln\left(\frac{\delta}{r_0} + \sqrt{\frac{\delta^2}{r_0^2} + \theta^2}\right) - \ln\left(\sqrt{\frac{\delta^2}{r_0^2} + \theta^2} - \frac{\delta}{r_0}\right) \xrightarrow{\theta\to 0} -\ln\theta^2. \tag{2.56}$$

The integral in the right side of Eq. (2.54) can be obtained readily:

$$\int_0^h rUF_n(z)\,\mathrm{d}z \xrightarrow{\theta\to 0} -\frac{\mathrm{i}I\,\mathrm{d}lF_n(z_s)}{4\pi\omega\varepsilon_0}\ln\theta^2. \tag{2.57}$$

When the observation point is close to the source, namely, $\theta \to 0$, the Legendre function of the first order $P_\nu(\cos(\pi-\theta))$ is approximated as

$$P_\nu\big(\cos(\pi-\theta)\big) \xrightarrow{\theta\to 0} \frac{\sin\nu\pi}{\pi}\ln\theta^2. \tag{2.58}$$

Thus, the result becomes

$$\begin{aligned} A_n &= \frac{1}{N_n}\lim_{\theta\to 0}\frac{1}{P_\nu(\cos(\pi-\theta))}\int_0^h rUF_n(z)\,\mathrm{d}z = -\frac{\mathrm{i}I\,\mathrm{d}lF_n(z_s)}{4\omega\varepsilon_0 N_n\sin\nu\pi} \\ &= -\frac{\mathrm{i}I\,\mathrm{d}lF(z_s)}{2\omega\varepsilon_0 h\sin\nu\pi}\Lambda_n, \end{aligned} \tag{2.59}$$

where the excitation factor Λ_n is defined by

$$\Lambda_n = \frac{1}{1+\frac{\sin 2kc_n h}{2kc_n h}}. \tag{2.60}$$

Therefore, we have

$$U = -\frac{\mathrm{i}I\,\mathrm{d}l}{2hr\omega\varepsilon_0}\sum_{n=0}^{\infty}\frac{\Lambda_n}{\sin\nu\pi}F_n(z_s)F_n(z_r)P_\nu\big(\cos(\pi-\theta)\big). \tag{2.61}$$

2.2.3 Approximated Formulas of SLF Field

With the substitution of Eq. (2.61) into Eqs. (2.1)–(2.3), the formulas for the three components E_r, E_θ, and H_ϕ can be derived readily:

$$E_r = -\frac{\mathrm{i}I\,\mathrm{d}l}{2\omega\varepsilon_0 hr^2}\cdot\sum_{n=0}^{\infty}\frac{\Lambda_n\nu(\nu+1)}{\sin\nu\pi}F_n(z_s)F_n(z_r)P_\nu\big(\cos(\pi-\theta)\big), \tag{2.62}$$

$$E_\theta = -\frac{\mathrm{i}I\,\mathrm{d}l\eta}{2hr}\cdot\sum_{n=0}^{\infty}\Lambda_n F_n(z_s)\frac{\partial F_n(z_r)}{k\partial z}\frac{\partial P_\nu(\cos(\pi-\theta))}{\sin\nu\pi\partial\theta}, \tag{2.63}$$

$$H_\phi = \frac{I\,\mathrm{d}l}{2hr}\cdot\sum_{n=0}^{\infty}\Lambda_n F_n(z_s)F_n(z_r)\frac{\partial P_\nu(\cos(\pi-\theta))}{\sin\nu\pi\partial\theta}. \tag{2.64}$$

In general, the parameter ν has a large positive imaginary part. It follows that

$$\nu \approx kaS_n - \frac{1}{2}; \qquad \sin\nu\pi \approx \frac{1}{2}\mathrm{e}^{-\mathrm{i}(\nu\pi-\frac{\pi}{2})}. \tag{2.65}$$

In SLF range, when the angle θ is not close to 0 and π, the function $P_\nu(\cos(\pi-\theta))$ is approximated as follows:

$$P_\nu\big(\cos(\pi-\theta)\big) \approx \left(\frac{1}{2\pi\nu\sin\theta}\right)^{\frac{1}{2}}\exp\left[-\mathrm{i}\left(\nu+\frac{1}{2}\right)(\pi-\theta)+\mathrm{i}\frac{\pi}{4}\right]. \tag{2.66}$$

Then, the complete formulas for the components E_r, E_θ, and H_ϕ of the electromagnetic field of a VED in the Earth–ionosphere waveguide can be expressed in the following forms:

$$E_r = -\frac{I\,\mathrm{d}l\eta\mathrm{e}^{-\mathrm{i}\frac{\pi}{4}}}{h\sqrt{\lambda a\sin\theta}}\sum_{n=0}^{\infty}\Lambda_n S_n^{\frac{3}{2}}F_n(z_s)F_n(z_r)\mathrm{e}^{\mathrm{i}kaS_n\theta}, \tag{2.67}$$

$$E_\theta = -\frac{I\,\mathrm{d}l\eta\mathrm{e}^{\mathrm{i}\frac{\pi}{4}}}{kh\sqrt{\lambda a\sin\theta}}\sum_{n=0}^{\infty}\Lambda_n S_n^{\frac{1}{2}}F_n(z_s)F_n'(z_r)\mathrm{e}^{\mathrm{i}kaS_n\theta}, \tag{2.68}$$

$$H_\phi = \frac{I\,\mathrm{d}l\mathrm{e}^{-\mathrm{i}\frac{\pi}{4}}}{h\sqrt{\lambda a\sin\theta}}\sum_{n=0}^{\infty}\Lambda_n S_n^{\frac{1}{2}}F_n(z_r)F_n(z_s)\mathrm{e}^{\mathrm{i}kaS_n\theta}. \tag{2.69}$$

Letting

$$E_0 = -\frac{I\,\mathrm{d}l\eta}{\lambda}\frac{\mathrm{e}^{\mathrm{i}ka\theta}}{a\theta}\ (\mathrm{V/m}) = -\frac{\mathrm{e}^{\mathrm{i}ka\theta}}{a\theta}300\sqrt{P_{\mathrm{kW}}}\ (\mathrm{mV/m}), \tag{2.70}$$

the approximated formula for the component E_r is rewritten as follows:

$$E_r = E_0\sqrt{\frac{d/a}{\sin(d/a)}}\frac{\sqrt{d/\lambda}}{h/\lambda}\mathrm{e}^{-\mathrm{i}kd-\mathrm{i}\frac{\pi}{4}}\sum_{n=0}^{\infty}\Lambda_n F_n(z_s)F_n(z_r)S_n^{3/2}\mathrm{e}^{\mathrm{i}kS_nd}, \tag{2.71}$$

where $d = a\theta$ is the propagation distance along the Earth's surface, and P_{kW} is the power in kW. Obviously, the approximated formulas for E_θ and H_ϕ can also be written readily.

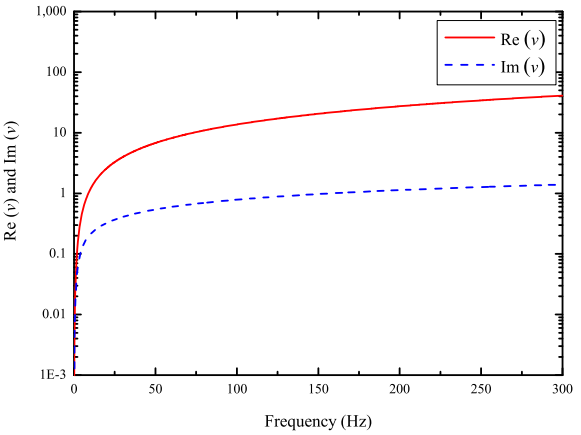

Fig. 2.1 The real and imaginary parts of ν versus the operating frequency

2.2.4 New Algorithm for ELF Field

In the whole ELF range, even in the lower end of SLF range, the wavelength λ is very long, which can be compared with the Earth's circumference. In other words, the parameter ka will be small. From $\nu(\nu+1) = k^2a^2S_n^2$, we find that the eigenvalue ν no longer satisfies the condition of $\nu \gg 1$. The eigenvalue ν of the zero-order TM wave is computed and shown in Fig. 2.1. It is seen that the eigenvalue does not satisfy $\nu \gg 1$ below 50 Hz. The Legendre function of the first kind $P_\nu(\cos(\pi-\theta))$ should not be evaluated by using its asymptotic formula in Eq. (2.29). In what follows, we will attempt to outline a new algorithm for evaluating the Legendre function of the first kind $P_\nu(\cos(\pi-\theta))$ (Peng et al. 2012).

In order to analyze quantitatively the ELF field in the Earth–ionosphere cavity, it is necessary to evaluate accurately the function $P_\nu(\cos(\pi-\theta))$. Generally, the eigenvalue ν is a complex number, and the Legendre function of the first kind $P_\nu(\cos(\pi-\theta))$ can be represented in the following form:

$$P_\nu\big(\cos(\pi-\theta)\big) = -\frac{\sin\nu\pi}{\pi}\sum_{n=0}^{\infty} P_n(\cos\theta)\frac{2n+1}{n(n+1)-\nu(\nu+1)}. \tag{2.72}$$

Another form of the function $P_\nu(\cos\theta)$ is expressed as Gradshteyn and Ryzhik (1980)

$$P_\nu(\cos\theta) = \frac{2}{\pi}\int_0^\theta \frac{\cos[(\nu+0.5)t]}{\sqrt{2(\cos t-\cos\theta)}}\,\mathrm{d}t. \tag{2.73}$$

Letting

$$\Phi(\nu,\theta) = \frac{1}{\sin\nu\pi}P_\nu\big(\cos(\pi-\theta)\big), \tag{2.74}$$

by using the following relation:

$$P'_{\nu}(z) = \frac{\nu}{z^2-1}\big[zP_{\nu}(z) - P_{\nu-1}(z)\big], \tag{2.75}$$

we write

$$\frac{\partial}{\partial\theta}\Phi(\nu,\theta) = \frac{\nu}{\sin\theta}\big[\Phi(\nu,\theta)\cos\theta - \Phi(\nu-1,\theta)\big]. \tag{2.76}$$

In practical numerical calculations, the function $\Phi(\nu,\theta)$ can be expressed in the integrated form

$$\Phi(\nu,\theta) = \frac{2}{\pi}\int_0^{\pi-\theta} \frac{M(\nu,t)}{\sqrt{2[\cos t - \cos(\pi-\theta)]}}\,\mathrm{d}t, \tag{2.77}$$

where

$$M(\nu,t) = \begin{cases} M_1(\nu,t); & 0 < \mathrm{Im}(\nu) \le 0.75, \\ M_2(\nu,t); & \mathrm{Im}(\nu) > 0.75, \end{cases} \tag{2.78}$$

and

$$M_1(\nu,t) = \frac{\cos(\nu+0.5)t}{\sin(\nu\pi)}, \tag{2.79}$$

$$\begin{aligned} M_2(\nu,t) = -\mathrm{i}\Bigg\{&\exp\bigg[\mathrm{i}\Big(\mathrm{Re}(\nu)t + \mathrm{Re}(\nu)\pi + \frac{t}{2}\Big)\bigg] \\ &\times \exp\big[-\mathrm{Im}(\nu)(\pi+t)\big] + \exp\big[-\mathrm{Im}(\nu)(\pi-t)\big] \\ &\times \exp\bigg[-\mathrm{i}\Big(\mathrm{Re}(\nu)t - \mathrm{Re}(\nu)\pi + \frac{t}{2}\Big)\bigg]\Bigg\}. \end{aligned} \tag{2.80}$$

Due to the singularity at $t = \pi - \theta$ existing in the integral Kernel function in Eq. (2.77), the function $\Phi(\nu,\theta)$ can be divided into two parts. We write

$$\Phi(\nu,\theta) = I_1 + I_2, \tag{2.81}$$

where

$$I_1 = \int_0^{\pi-\theta-\delta} \frac{M(\nu,t)}{\sqrt{2[\cos t - \cos(\pi-\theta)]}}\,\mathrm{d}t, \tag{2.82}$$

$$I_2 = \int_{\pi-\theta-\delta}^{\pi-\theta} \frac{M(\nu,t)}{\sqrt{2[\cos t - \cos(\pi-\theta)]}}\,\mathrm{d}t. \tag{2.83}$$

It is noted that the first integral I_1 can be evaluated readily by using the trapezoidal or Simpson's numerical integration method. For the second integral I_2, with

the change of the variable $\pi - \theta - s = t$, it follows that

$$I_2 = \int_0^{\delta} \frac{M(\nu, \pi - \theta - s)}{2\sqrt{\sin(\pi - \theta - \frac{s}{2})\sin(\frac{s}{2})}} \mathrm{d}s. \tag{2.84}$$

When $\delta \to 0$, it is seen that the function $\frac{M(\nu,\pi-\theta-s)}{2\sqrt{\sin(\pi-\theta-\frac{s}{2})}}$ is approximately a constant in the interval $[0, \delta]$. Then, we have

$$\begin{aligned} I_2 &\approx \frac{1}{4}\left[\frac{M(\nu, \pi - \theta)}{\sin(\pi - \theta)} + \frac{M(\nu, \pi - \theta - \delta)}{\sin(\pi - \theta - \frac{\delta}{2})}\right] \cdot \int_0^{\delta} \sqrt{\frac{2}{s}}\, \mathrm{d}s \\ &= \sqrt{\frac{\delta}{2}}\left[\frac{M(\nu, \pi - \theta)}{\sin(\pi - \theta)} + \frac{M(\nu, \pi - \theta - \delta)}{\sin(\pi - \theta - \frac{\delta}{2})}\right]. \end{aligned} \tag{2.85}$$

By now, the approximated formula has been derived for the Legendre function of the first order $P_\nu(\cos(\pi - \theta))$ in the case of $\nu < 1$. In whole ELF range, even in the lower end of SLF range, the three non-zero components E_r, E_θ, and H_ϕ can be evaluated accurately by using Eqs. (2.88)–(2.90).

Additionally, by using the Legendre polynomial expansion of $P_\nu(\cos(\pi - \theta))$, the Legendre function $P_\nu(\cos(\pi - \theta))$ can also be calculated accurately. We write

$$\begin{aligned} \Phi_1(\nu, \theta) &= \frac{P_\nu(\cos(\pi - \theta))}{\sin \nu\pi} \\ &= -\frac{1}{\pi}\sum_{n=0}^{\infty} P_n(\cos\theta)\frac{2n+1}{n(n+1) - \nu(\nu+1)}. \end{aligned} \tag{2.86}$$

As shown in Fig. 2.2, the ratios of the calculated results by using the series algorithm of Eq. (2.86) and those by using the numerical integrated algorithm of Eq. (2.81) are carried out at $n = 100$, 200, and 500, respectively. It is seen that the calculated results $\Phi_1(\nu, \theta)$ by using the series algorithm move closer to the corresponding approximated results $\Phi(\nu, \theta)$ by using the approximated algorithm proposed in this section when the parameter n increases. When n is larger than 200, the results by using the series algorithm are in agreement with those by the numerical integrated algorithm. Obviously, the numerical integrated algorithm in evaluating the Legendre function works more quickly and easily.

In earlier works for the SLF field computation, the asymptotic expansion for the function $P_\nu(\cos(\pi - \theta))$ is usually employed by Eq. (2.29). We write

$$\begin{aligned} \Phi_2(\nu, \theta) &= \frac{P_\nu(\cos(\pi - \theta))}{\sin \nu\pi} \\ &\approx \frac{1}{\sin \nu\pi}\sqrt{\frac{2}{\pi\nu\sin\theta}}\cos\left[\left(\nu + \frac{1}{2}\right)(\pi - \theta) - \frac{\pi}{4}\right]. \end{aligned} \tag{2.87}$$

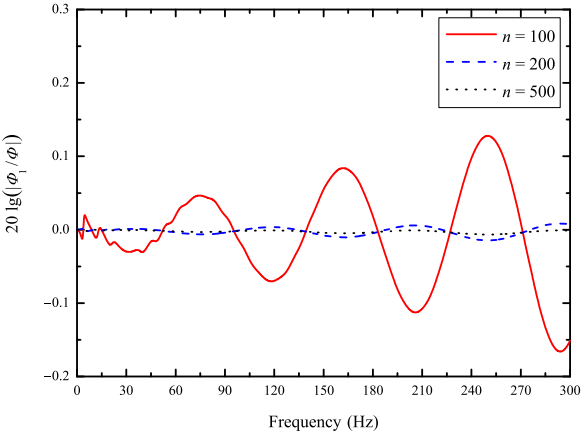

Fig. 2.2 The ratio $\Phi_1(\nu,\theta)/\Phi(\nu,\theta)$ versus the operating frequency

Compared with the other two algorithms, the numerical integrated algorithm has the merits of high accuracy and efficiency, which is suitable for the field computations in ELF range and the lower end of SLF range, which is below 50 Hz or so. Thus, the complete formulas for the field components in Eqs. (2.67)–(2.69) are rewritten in the following forms:

$$E_r = -\frac{\mathrm{i}I\,\mathrm{d}l}{2\omega\varepsilon_0 hr^2}\cdot\sum_{n=0}^{\infty}\left[\Lambda_n(kaS_n)^2\cdot F_n(z_r)F_n(z_s)\Phi(\nu,\theta)\right], \tag{2.88}$$

$$E_\theta = -\frac{\mathrm{i}I\,\mathrm{d}l}{2\omega\varepsilon_0 hr}\cdot\sum_{n=0}^{\infty}\left\{\Lambda_n F_n(z_s)\frac{\mathrm{d}F_n(z_r)}{\mathrm{d}z}\right.$$
$$\left.\times\frac{\nu}{\sin\theta}\left[\Phi(\nu,\theta)\cos\theta-\Phi(\nu-1,\theta)\right]\right\}, \tag{2.89}$$

$$H_\phi = \frac{I\,\mathrm{d}l}{2hr}\cdot\sum_{n=0}^{\infty}\left\{\Lambda_n F_n(z_s)F_n(z_r)\right.$$
$$\left.\times\frac{\nu}{\sin\theta}\left[\Phi(\nu,\theta)\cos\theta-\Phi(\nu-1,\theta)\right]\right\}. \tag{2.90}$$

Evidently, the field components for the ELF range can be evaluated accurately by using Eqs. (2.88)–(2.90).

We assume that the Earth's radius is taken as $a = 6{,}370$ km, the current moment of the dipole is $I\,\mathrm{d}l = 1$ A·m, the ground conductivity is $\sigma_g = 10^{-4}$ S/m, the ionospheric conductivity is $\sigma_i = 10^{-5}$ S/m, and the ionospheric equivalent reflection height is $h = 70$ km. By using Eqs. (2.88)–(2.90), the magnitudes of the three components E_r, E_θ, and H_ϕ are computed at $f = 1$ Hz, 3 Hz, 5 Hz, 10 Hz, 20 Hz, and 30 Hz, and shown in Figs. 2.3, 2.4, 2.5, respectively. From the above computations, the discussions are carried out and conclusions are drawn as follows:

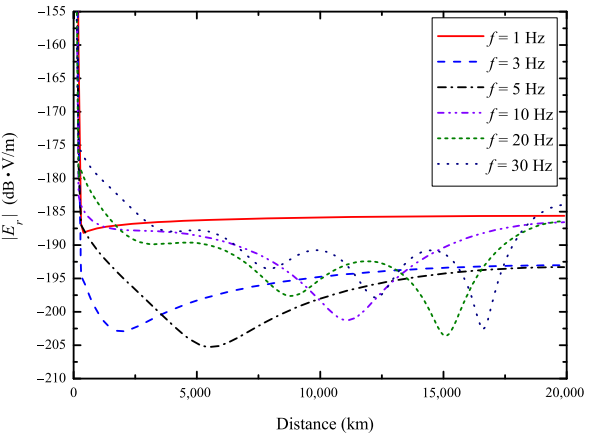

Fig. 2.3 The magnitudes of E_r versus the propagation distances at $f = 1$ Hz, 3 Hz, 5 Hz, 10 Hz, 20 Hz, and 30 Hz

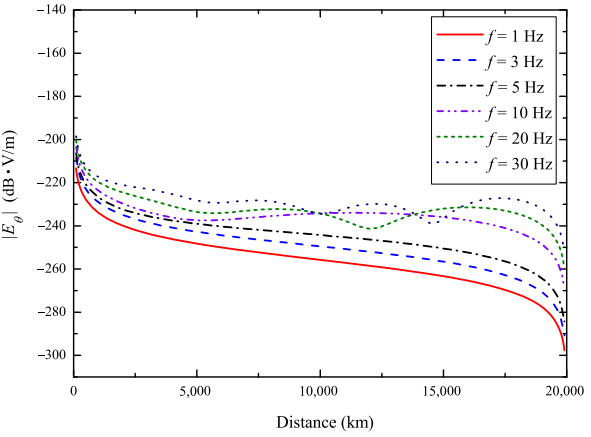

Fig. 2.4 The magnitudes of E_θ versus the propagation distances at $f = 1$ Hz, 3 Hz, 5 Hz, 10 Hz, 20 Hz, and 30 Hz

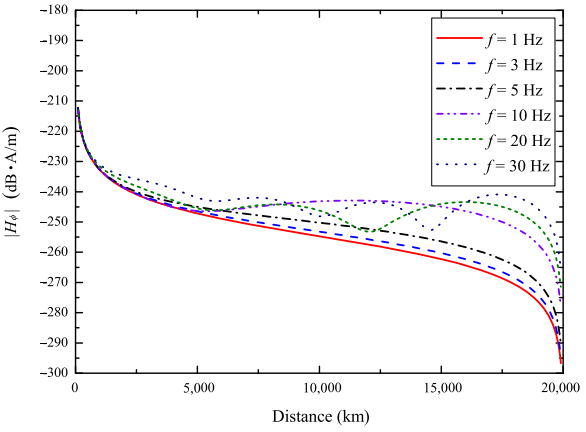

Fig. 2.5 The magnitudes of H_ϕ versus the propagation distances at $f = 1$ Hz, 3 Hz, 5 Hz, 10 Hz, 20 Hz, and 30 Hz

- When the observation point is close to the antipole of the dipole source, the multipath effects should be considered. The interference phenomenon is resulted by the two waves traveling along the small and large circle paths. The higher the operating frequency is, the more severely the field strength by the interference fluctuates. The smaller the distance from the observation point to the antipole, the more smoothing the field strength by the interference fluctuates.
- With the decrease of the operating frequency, the magnitude of the component E_r, which is generated by a VED in the Earth–ionosphere cavity, becomes relatively "flat". When the operating frequency is below 1 Hz, the magnitude tends approximately to a constant at a distance larger than 1,000 km. In the range below 50 Hz, only the quasi-TEM wave can propagate in the Earth–ionosphere cavity. When $\nu \to 0$, we have $P_\nu(\cos(\pi - \theta)) \to 1$, $\phi(\nu, \theta) \to \frac{1}{\nu\pi}$. Namely, the magnitude becomes stable, which varies little with the propagation distance. In what follows, we will attempt to give the physical explanations as follows: In the range below 50 Hz, the wavelength is comparable to the Earth's circumference, and the electromagnetic wave in the Earth–ionosphere cavity exists in the form of "stationary wave". Furthermore, at the frequency range below 1 Hz, the wavelengths can be a dozen or dozens of the Earth's circumference. This means that the phase differences at different propagation paths are small, and the total field is approximately equal to the sum of the electric fields with the same phases on different propagation paths. Therefore, the interference phenomenon is gradually disappearing and the total field becomes stable in the zones which are far away from the source point.
- Due to the spherically symmetry, the propagation characteristics of E_θ and H_ϕ are also similar. Moreover, the magnitudes of the field components E_θ and H_ϕ are equal to 0 at the antipole of the dipole source and decrease drastically in the zone near the antipole.

2.3 SLF/ELF Field of VMD in the Earth–Ionosphere Waveguide/Cavity

In practical applications, it is impossible to employ a VMD to generate TE waves in SLF/ELF ranges. In order to investigate the electromagnetic waves generated by an HED, it is necessary to analyze the propagation characteristics for both TM and TE waves. It is well known that a VMD is a typical excitation source for TE waves. In this section, we will examine the electromagnetic field of VMD in the Earth–ionosphere waveguide or cavity.

If the excitation source in the preceding section is replaced by a VMD with its moment $M = I\,\mathrm{d}a$, and $\mathrm{d}a$ is the area of the loop, the non-zero components E_ϕ, H_r, and H_θ, which the TE waves radiated by a VMD, are represented in the following

forms:

$$E_\phi = -\frac{\mathrm{i}\omega\mu}{r}\frac{\partial}{\partial\theta}(Vr), \tag{2.91}$$

$$H_r = \left(\frac{\partial}{\partial r^2} + k^2\right)(Vr), \tag{2.92}$$

$$H_\theta = \frac{1}{r}\frac{\partial^2}{\partial\theta\partial r}(Vr), \tag{2.93}$$

where the potential function V satisfies the scalar Helmholtz equation,

$$\left(\nabla^2 + k^2\right)V = 0. \tag{2.94}$$

The solution for V is represented in the form

$$V = \frac{1}{r}G(r)\Phi(\theta). \tag{2.95}$$

In the same manner as in the preceding section, we obtain readily:

$$\Phi(\theta) = P_\nu\big(\cos(\pi - \theta)\big), \tag{2.96}$$

$$G(r) = A\exp\left[-\mathrm{i}k\int_0^z \left(C^2 + \frac{2z}{a}S^2\right)^{1/2}\mathrm{d}z\right] + B\exp\left[\mathrm{i}k\int_0^z \left(C^2 + \frac{2z}{a}S^2\right)^{1/2}\mathrm{d}z\right], \tag{2.97}$$

where the relations between both the parameters S and C and the eigenvalue ν are represented as follows:

$$S^2 = \frac{\nu(\nu+1)}{k^2a^2}; \qquad C^2 = 1 - S^2. \tag{2.98}$$

From the boundary conditions

$$\left.\frac{E_\phi}{\eta_1 H_\theta}\right|_{r=a} = \Delta_g, \qquad \left.\frac{E_\phi}{\eta_1 H_\theta}\right|_{r=a+h} = -\Delta_i, \tag{2.99}$$

we rewrite

$$\left.\frac{1}{V}\frac{\partial V}{\partial r}\right|_{r=a} = -\frac{\mathrm{i}k}{\Delta_g}, \tag{2.100}$$

$$\left.\frac{1}{V}\frac{\partial V}{\partial r}\right|_{r=a+h} = \frac{\mathrm{i}k}{\Delta_i}. \tag{2.101}$$

Substituting Eq. (2.95) into Eqs. (2.100) and (2.101), the modal equation for TE waves is obtained readily. It is

$$R_g^h R_i^h \exp\left[2\mathrm{i}k\int_0^h \left(C_m^2+\frac{2z}{a}S_n^2\right)^{1/2}\mathrm{d}z\right]=\mathrm{e}^{2\mathrm{i}(m-1)\pi}, \tag{2.102}$$

where

$$R_g^h=\left(C_m-\Delta_g^{-1}\right)\left(C_m+\Delta_g^{-1}\right)^{-1}, \tag{2.103}$$

$$R_i^h=\left(C_m'-\Delta_i^{-1}\right)\left(C_m'+\Delta_i^{-1}\right)^{-1}, \tag{2.104}$$

$$C_m'=\left(C_m^2+\frac{2h}{a}S_m^2\right)^{1/2}\approx C_m. \tag{2.105}$$

If C_m ($m = 1, 2, 3, \ldots$) are the roots of the modal equation (2.102), the height-gain functions $G_m(z)$ can be represented in the following form:

$$G_m(z)=\frac{1}{(1+R_g^h)}\left\{\exp\left[-\mathrm{i}k\int_0^z\left(C_m^2+\frac{2t}{a}S_m^2\right)^{1/2}\mathrm{d}t\right]\right.$$
$$\left.+R_g^h\exp\left[\mathrm{i}k\int_0^z\left(C_m^2+\frac{2t}{a}S_m^2\right)^{1/2}\mathrm{d}t\right]\right\}. \tag{2.106}$$

In SLF/ELF ranges, we find $1/\Delta_g \gg C_m$ and $1/\Delta_i \gg C_m$. Then, the reflection coefficients R_g^h and R_i^h can be simplified as follows:

$$R_g^h\approx-\exp(-2C_m\Delta_g), \tag{2.107}$$

$$R_i^h\approx-\exp(-2C_m\Delta_i). \tag{2.108}$$

By solving the modal equation (2.102), the roots C_m ($m = 1, 2, 3, \ldots$) are approximated by

$$C_m\approx\frac{m\pi}{kh}\left(1+\mathrm{i}\frac{\Delta_g+\Delta_i}{kh}\right)^{-1}, \tag{2.109}$$

$$S_m=\left(1-C_m^2\right)^{1/2}. \tag{2.110}$$

Similar to those for TM waves, the different modes for TE waves are orthogonal each other. Then, we obtain readily:

$$N_{m\mu}=\int_0^h G_m(z)G_\mu(z)\,\mathrm{d}z=0;\quad \text{when } \mu\neq m, \tag{2.111}$$

and

$$N_{m\mu} = \int_0^h G_m(z)G_\mu(z)\,\mathrm{d}z = \lim_{S_\mu \to S_m} \frac{G'_m(h)G_\mu(h) - G_m(h)G'_\mu(h)}{k^2(S_m^2 - S_\mu^2)}$$

$$= -\frac{4R_g^h k^2 C'_m \frac{\partial H}{\partial S_m} - 2\mathrm{i}kC'_m \frac{\partial R_g^h}{\partial S_m}}{2k^2 S_m (1+R_g^h)^2}$$

$$- \frac{\mathrm{i}k\frac{\partial C'_m}{\partial S_m}[\exp(-2\mathrm{i}kH) - (R_g^h)^2\exp(2\mathrm{i}kH)]}{2k^2 S_m(1+R_g^h)^2}; \quad \text{when } \mu = m, \tag{2.112}$$

where

$$H = \int_0^h \left(C_m^2 + \frac{2z}{a}S_m^2\right)^{1/2}\mathrm{d}z = \frac{a}{3S_m^2}\left(C_m'^{\,3} - C_m^3\right). \tag{2.113}$$

After algebraic manipulation, the factor N_m is written in the following form:

$$N_m = \frac{4R_g^h}{(1+R_g^h)^2}\frac{aC'_m}{3S_m^4}\left\{C_m'^{\,3} - C_m^3 + \frac{3S_m^2}{2}\left[C'_m\left(1-\frac{2h}{a}\right) - C_m\right]\right\}$$

$$- \frac{2\mathrm{i}C'_m\Delta_g}{kC_m(1+C_m\Delta_g)^2(1+R_g^h)^2}$$

$$+ \frac{\mathrm{i}(1-\frac{2h}{a})[\exp(-2\mathrm{i}kH) - (R_g^h)^2\exp(2\mathrm{i}kH)]}{2kC'_m(1+R_g^h)^2}. \tag{2.114}$$

In SLF/ELF ranges, R_g^h is close to -1. Then, we have

$$1 + R_g^h = \frac{2C_m\Delta_g}{1+C_m\Delta_g}. \tag{2.115}$$

When $C_m \gg \frac{2h}{a}$, we get

$$C_m'^{\,3} - C_m^3 + \frac{3}{2}S_m^2\left[C'_m\left(1-\frac{2h}{a}\right) - C_m\right] \approx \frac{3hS_m^4}{2aC_m}. \tag{2.116}$$

Then, the factor N_m can be simplified as follows:

$$N_m = -\frac{h}{2\Delta_g^2 C_m^2}\left[1 - \frac{\sin 2kC_m h}{2kC_m h} - \Delta_g^2 C_m^2\left(1 + \frac{\sin 2kC_m h}{2kC_m h}\right)\right.$$

$$\left. - \mathrm{i}\frac{\Delta_g}{kh}(\cos 2kC_m h - 1)\right]. \tag{2.117}$$

By now, the potential function V can be written in the form of

$$V = \frac{1}{r}\sum_{m=1}^{\infty} A_m G_m(z) P_\nu\big(\cos(\pi-\theta)\big). \tag{2.118}$$

Correspondingly, the component E_ϕ is expressed as follows:

$$E_\phi = -\frac{\mathrm{i}\omega\mu}{r}\sum_{m}^{\infty} A_m G_m(z)\frac{\partial}{\partial\theta} P_\nu\big(\cos(\pi-\theta)\big). \tag{2.119}$$

By multiplying the factor $rG_m(z)\,\mathrm{d}z$ on both sides of Eq. (2.119), and integrating from 0 to h for z, we have

$$-\mathrm{i}\omega\mu A_m N_m \frac{\partial}{\partial\theta} P_\nu\big(\cos(\pi-\theta)\big) = \int_0^h rE_\phi G_m(z)\,\mathrm{d}z. \tag{2.120}$$

Close to the dipole source, we obtain readily:

$$\lim_{\theta\to 0} 2\pi r_s\theta E_\phi(r_s,\theta) = \mathrm{i}\omega\mu_0 \iint H_z(r_s,\theta)\,\mathrm{d}a = \mathrm{i}\omega\mu_0\delta(r-r_s)I\,\mathrm{d}a, \tag{2.121}$$

where the moment of the dipole source is $I\,\mathrm{d}a$, and $\mathrm{d}a$ is the loop area. It is noted that Eq. (2.120) is satisfied for any angle θ. Obviously, from Eq. (2.121), we have

$$\lim_{\theta\to 0}\int_0^h rE_\phi G_m(z)\,\mathrm{d}z = \frac{\mathrm{i}\omega\mu_0}{2\pi\theta} I\,\mathrm{d}aG_m(z_s). \tag{2.122}$$

Thus, it follows that

$$A_m = -\frac{I\,\mathrm{d}aG_m(z_s)}{2\pi N_m}\lim_{\theta\to 0}\left\{\theta\frac{\partial}{\partial\theta}P_\nu\big(\cos(\pi-\theta)\big)\right\}^{-1}. \tag{2.123}$$

By using the following asymptotic formula in the case of $\theta\to 0$:

$$P_\nu\big(\cos(\pi-\theta)\big) \approx \frac{2\sin\nu\pi}{\pi}\ln\theta, \tag{2.124}$$

we have

$$\lim_{\theta\to 0}\theta\frac{\partial}{\partial\theta}P_\nu\big(\cos(\pi-\theta)\big) \approx \frac{2\sin\nu\pi}{\pi}. \tag{2.125}$$

Thus, the coefficient A_m can be determined readily. We write

$$A_m = -\frac{I\,\mathrm{d}aG_m(z_s)}{4\sin\nu\pi N_m}. \tag{2.126}$$

The three non-zero components E_ϕ, H_r, and H_θ can be expressed in the following forms:

$$E_\phi = \frac{\mathrm{i}\omega\mu_0 I\,\mathrm{d}a}{4r}\sum_m^\infty \frac{G_m(z_s)}{\sin(\mu\pi)N_m}G_m(z_r)\frac{\partial}{\partial\theta}P_\nu\big(\cos(\pi-\theta)\big), \tag{2.127}$$

$$H_r = -\frac{I\,\mathrm{d}a}{4r^2}\sum \frac{\nu(\nu+1)}{\sin(\mu\pi)N_m}G_m(z_s)G_m(z_r)P_\nu\big(\cos(\pi-\theta)\big), \tag{2.128}$$

$$H_\theta = -\frac{I\,\mathrm{d}a}{4r}\sum \frac{G_m(z_s)}{\sin(\mu\pi)N_m}\frac{\partial}{\partial z}G_m(z_r)\frac{\partial}{\partial\theta}P_\nu\big(\cos(\pi-\theta)\big). \tag{2.129}$$

For TE waves in SLF/ELF ranges, because of $\nu(\nu+1)=k^2a^2S_m^2$, in general the factor S_m is a purity imaginary number. Thus the parameter $\nu+\frac{1}{2}$ is a complex number with a large imaginary part. Then, in the case that the angle θ is not close to 0 and π, we have

$$\frac{P_\nu(\cos(\pi-\theta))}{\sin(\nu\pi)} \approx -\sqrt{\frac{2}{\pi kaS_m\sin\theta}}\cdot\exp\left(\mathrm{i}kaS_m\theta+\frac{\mathrm{i}\pi}{4}\right), \tag{2.130}$$

$$\frac{\partial P_\nu(\cos(\pi-\theta))}{\sin(\nu\pi)\partial\theta} \approx -\mathrm{i}\sqrt{\frac{2kaS_m}{\pi\sin\theta}}\cdot\exp\left(\mathrm{i}kaS_m\theta+\frac{\mathrm{i}\pi}{4}\right). \tag{2.131}$$

The three non-zero components E_ϕ, H_r, and H_θ for TE waves can be written as follows:

$$E_\phi = -\frac{I\,\mathrm{d}ak\eta}{h}\sqrt{\frac{1}{\lambda a\sin\theta}}\sum_{m=1}^\infty \Lambda_m G_m(z_s)G_m(z_r)S_m^{1/2}\mathrm{e}^{\mathrm{i}kaS_m\theta+\mathrm{i}\frac{\pi}{4}}, \tag{2.132}$$

$$H_r = -\frac{I\,\mathrm{d}ak}{h}\sqrt{\frac{1}{\lambda a\sin\theta}}\sum_{m=1}^\infty \Lambda_m G_m(z_s)G_m(z_r)S_m^{3/2}\mathrm{e}^{\mathrm{i}kaS_m\theta+\mathrm{i}\frac{\pi}{4}}, \tag{2.133}$$

$$H_\theta = -\frac{\mathrm{i}I\,\mathrm{d}ak}{h}\sqrt{\frac{1}{\lambda a\sin\theta}}\sum_{m=1}^\infty \Lambda_m G_m(z_s)S_m^{1/2}\frac{\partial G_m(z_r)}{k\partial z}\mathrm{e}^{\mathrm{i}kaS_m\theta+\mathrm{i}\frac{\pi}{4}}, \tag{2.134}$$

where the excitation factor Λ_m for TE waves is defined by

$$\Lambda_m = \Delta_g^2C_m^2\bigg[1-\frac{\sin 2kC_mh}{2kC_mh}-\Delta_g^2C_m^2\left(1+\frac{\sin 2kC_mh}{2kC_mh}\right) -\mathrm{i}\frac{\Delta_g}{kh}(\cos 2kC_mh-1)\bigg]^{-1}. \tag{2.135}$$

In general, in SLF/ELF ranges, the normalized surface impedance Δ_g is very small, so that the excitation efficiency of VMD is very low.

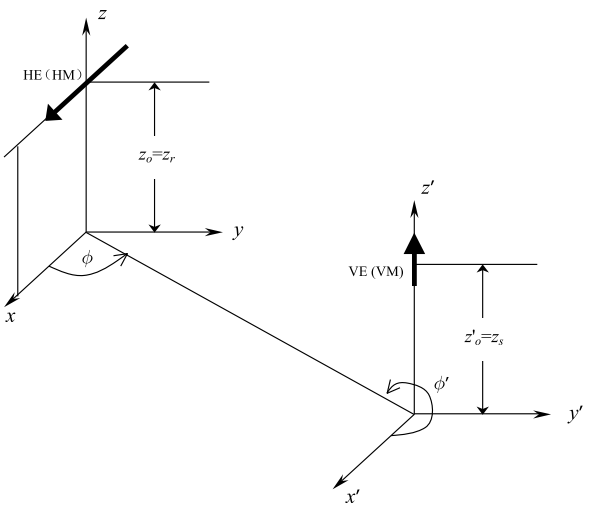

Fig. 2.6 The diagram for the geometric relation between the transmitting and receiving antennas

2.4 SLF/ELF Field of HED in the Earth–Ionosphere Waveguide/Cavity

In practical applications, a SLF/ELF radiation source is usually employed a horizontal linear antenna. So that it is necessary to investigate SLF/ELF electromagnetic field of an HED in the anisotropic Earth–ionosphere waveguide or cavity. In the preceding sections, the electromagnetic field of a VED and that of VMD are addressed, respectively. The complete formulas can be derived for the electromagnetic field of an HED in the presence of the Earth–ionosphere cavity by the reciprocity theorem (Wait 1970; Galejs 1972a). It is stated that the voltage V_2 excited in antenna 2 by current I_1 of antenna 1 is equal to the voltage V_1 excited in antenna 1 by an identical current I_2 in antenna 2.

The geometry for a VED with its length $\mathrm{d}l^{\mathrm{ve}}$ at $z'_0 = z_s$ and an HED with its length $\mathrm{d}s^{\mathrm{he}}$ parallel to the x-axis at $z_0 = z_r$ are illustrated in Fig. 2.6, where the subscripts r and s refer to the observation point and dipole source, respectively. It is known that the magnitude of the voltage V^{he} excited in HED is maximum when $E^{\mathrm{ve}}_{\rho'}$ is parallel to the $\hat{x}$ axis ($\phi = 0$ and π). Then, we have

$$V^{\mathrm{he}} = -E^{\mathrm{ve}}_{\rho'}\left(z'_0 = z_s, z_0 = z_r\right)\cos\phi\,\mathrm{d}s^{\mathrm{he}}, \tag{2.136}$$

where the superscripts *ve* and *he* refer to the VEDs and HEDs, respectively. Similarly, the magnitude of the voltage V^{ve} in the VED is contributed by the field component E^{he}_z excited by the horizontal electric dipole. We write

$$V^{\mathrm{ve}} = E^{\mathrm{he}}_z\left(z_0 = z_s, z'_0 = z_r\right)\mathrm{d}l^{\mathrm{ve}}. \tag{2.137}$$

With $\mathrm{d}s^{\mathrm{he}} = \mathrm{d}l^{\mathrm{ve}}$, from Eqs. (2.136) and (2.137), it follows that

$$E_z^{\mathrm{he}}\left(z_0 = z_s, z_0' = z_r\right) = -E_{\rho'}^{\mathrm{ve}}\left(z_0' = z_s, z_0 = z_r\right)\cos\phi. \tag{2.138}$$

Next, we consider the geometry for a VMD with its loop area da^{vm} parallel to the z'-axis at $z_0' = z_s$ and an HED parallel to the x-axis at $z_0 = z_r$, which is shown in Fig. 2.6. The magnitude of voltage in the HED V^{he} by the VMD is represented as follows:

$$V^{\mathrm{he}} = E_{\phi'}^{\mathrm{vm}}\left(z_0' = z_s, z_0 = z_r\right)\sin\phi\,\mathrm{d}s^{\mathrm{he}}, \tag{2.139}$$

where the superscript vm refers to the VMD. The magnitude of voltage V^{vm} in the VMD is contributed by the component H_z^{he} excited by the HED with the same current. We write

$$V^{\mathrm{vm}} = \mathrm{i}\omega\mu_0 H_z^{\mathrm{he}}\left(z_0 = z_s, z_0' = z_r\right)\mathrm{d}a^{\mathrm{vm}}. \tag{2.140}$$

With $V^{\mathrm{he}} = V^{\mathrm{vm}}$, from Eqs. (2.139) and (2.140), it follows that

$$H_z^{\mathrm{he}}\left(z_0 = z_s, z_0' = z_r\right) = \frac{1}{\mathrm{i}\omega\mu_0}E_\phi\left(z_0' = z_s, z_0 = z_r\right)\sin\phi\frac{\mathrm{d}s^{\mathrm{he}}}{\mathrm{d}a^{\mathrm{vm}}}. \tag{2.141}$$

For spherical coordinates the z and ρ components are replaced by the r and θ components, respectively. With Eq. (2.138), and considering that the sign should be changed for θ derivatives when interchanging the coordinates of the receiver and source, it follows that

$$\begin{aligned} E_r^{\mathrm{he}}(r,\theta,\phi) = &-\frac{\mathrm{i}I\,\mathrm{d}s^{\mathrm{he}}\eta\cos\phi}{2ha} \\ &\times\sum_{n=0}^{\infty}\Lambda_n^e F_n(z_r)\frac{\partial F_n(z_s)}{k\partial z}\frac{\partial P_\nu(\cos(\pi-\theta))}{\sin\nu\pi\partial\theta}. \end{aligned} \tag{2.142}$$

Similarly, with the substitution of Eq. (2.132) into Eq. (2.141), it follows that

$$H_r^{\mathrm{he}}(r,\theta,\phi) = \frac{I\,\mathrm{d}s^{\mathrm{he}}\sin\phi}{2ha}\sum_{m=1}^{\infty}\Lambda_m^h G_m(z_r)G_m(z_s)\frac{\partial P_\mu(\cos(\pi-\theta))}{\sin\mu\pi\partial\theta}. \tag{2.143}$$

Here $F_n(z)$ and $G_m(z)$ refer to the height-gain function for TM_n wave and that for TE_m wave, respectively. The excitation factor Λ_n^e for TM_n wave and the excitation factor Λ_m^h for TE_m wave are represented by (2.60) and (2.135), respectively. We rewrite

$$\Lambda_n^e = \frac{1}{1+\frac{\sin 2kC_n h}{2kC_n h}}, \tag{2.144}$$

$$\Lambda_m^h = \Delta_g^2 C_m^2 \Bigg[1 - \frac{\sin 2kC_m h}{2kC_m h} - \Delta_g^2 C_m^2 \left(1 + \frac{\sin 2kC_m h}{2kC_m h} \right) - \mathrm{i}\frac{\Delta_g}{kh}(\cos 2kC_m h - 1) \Bigg]^{-1}. \tag{2.145}$$

From the expanded representations of Maxwell's equations in the spherical coordinate system, the components E_θ, E_ϕ, H_θ, and H_ϕ can be expressed in terms of E_r and H_r. We write

$$\left(k^2 + \frac{\partial^2}{\partial r^2} \right)(r \sin\theta H_\theta) = -\mathrm{i}\omega\varepsilon \frac{\partial}{\partial \phi} E_r + \sin\theta \frac{\partial^2}{\partial\theta \partial r} H_r, \tag{2.146}$$

$$\left(k^2 + \frac{\partial^2}{\partial r^2} \right)(r \sin\theta E_\phi) = \frac{\partial^2}{\partial\phi \partial r} E_r - \mathrm{i}\omega\mu_0 \sin\theta \frac{\partial}{\partial\theta} H_r, \tag{2.147}$$

$$\left(k^2 + \frac{\partial^2}{\partial r^2} \right)(r \sin\theta H_\phi) = \mathrm{i}\omega\varepsilon_0 \sin\theta \frac{\partial}{\partial\theta} E_r + \frac{\partial^2}{\partial\phi \partial r} H_r, \tag{2.148}$$

$$\left(k^2 + \frac{\partial^2}{\partial r^2} \right)(r \sin\theta E_\theta) = \sin\theta \frac{\partial^2}{\partial\theta \partial r} E_r + \mathrm{i}\omega\mu_0 \frac{\partial}{\partial\phi} H_r. \tag{2.149}$$

Taking into account the following relations:

$$\left(\frac{\partial^2}{\partial r^2} + k^2 \right) Z_n(z) = \frac{\nu(\nu+1)}{r^2} Z_n(z), \tag{2.150}$$

the complete formulas for the components E_θ^{he}, E_ϕ^{he}, H_θ^{he}, and H_ϕ^{he} can be written in the following forms:

$$H_\theta^{\mathrm{he}} = \frac{I\,\mathrm{d}s^{\mathrm{he}} \sin\phi}{2ha} \left\{ \frac{1}{ka \sin\theta} \sum_n \Lambda_n^e S_n^{-2} F_n(z_r) \frac{\partial F_n(z_s)}{k\partial z} \frac{\partial P_\nu(\cos(\pi - \theta))}{\sin \nu\pi \partial\theta} + \frac{1}{ka} \sum_m \frac{\Lambda_m^h G_m(z_s)}{S_m^2} \frac{\partial G_m(z_r)}{k\partial z} \frac{\partial^2 P_\mu(\cos(\pi - \theta))}{\sin \mu\pi \partial^2\theta} \right\}, \tag{2.151}$$

$$H_\phi^{\mathrm{he}} = \frac{I\,\mathrm{d}s^{\mathrm{he}} \cos\phi}{2ha} \left\{ \frac{1}{ka} \sum_n \Lambda_n^e S_n^{-2} F_n(z_r) \frac{\partial F_n(z_s)}{k\partial z} \frac{\partial^2 P_\nu(\cos(\pi - \theta))}{\sin \nu\pi \partial^2\theta} + \frac{1}{ka \sin\theta} \sum_m \frac{\Lambda_m^h G_m(z_s)}{S_m^2} \frac{\partial G_m(z_r)}{k\partial z} \frac{\partial P_\mu(\cos(\pi - \theta))}{\sin \mu\pi \partial\theta} \right\}, \tag{2.152}$$

$$E_\theta^{\mathrm{he}} = -\frac{\mathrm{i}I\,\mathrm{d}s^{\mathrm{he}} \eta \cos\phi}{2ha} \left\{ \frac{1}{ka} \sum_n \Lambda_n^e S_n^{-2} \frac{\partial F_n(z_r)}{k\partial z} \frac{\partial F_n(z_s)}{k\partial z} \frac{\partial^2 P_\nu(\cos(\pi - \theta))}{\sin \nu\pi \partial\theta^2} - \frac{1}{ka \sin\theta} \sum_m \Lambda_m^h G_m(z_s) G_m(z_r) S_m^{-2} \frac{\partial P_\mu[\cos(\pi - \theta)]}{\sin \mu\pi \partial\theta} \right\}, \tag{2.153}$$

$$E_{\phi}^{\mathrm{he}}=\frac{\mathrm{i}I\,\mathrm{d}s^{\mathrm{he}}\eta}{2ha}\sin\phi\left\{\frac{1}{ka\sin\theta}\sum_{n}\Lambda_{n}^{e}S_{n}^{-2}\frac{\partial F_{n}(z_{r})}{k\partial z}\frac{\partial F_{n}(z_{s})}{k\partial z}\frac{\partial P_{\nu}(\cos(\pi-\theta))}{\sin\nu\pi\partial\theta}\right.$$

$$\left.-\frac{1}{ka}\sum_{m}\Lambda_{m}^{h}G_{m}(z_{s})G_{m}(z_{r})S_{m}^{-2}\frac{\partial^{2}P_{\mu}(\cos(\pi-\theta))}{\sin\mu\pi\partial^{2}\theta}\right\}. \tag{2.154}$$

In SLF/ELF ranges, the horizontal antenna is usually placed on the ground. Then, we take $z_s=z_r=0$, $F_n(0)=G_m(0)=1$, $\frac{\partial F_n(z)}{k\partial z}|_{z=0}=-\mathrm{i}\Delta_g$, and $\frac{\partial G_m(z)}{k\partial z}|_{z=0}=-\frac{\mathrm{i}}{\Delta_g}$. We write

$$E_{r}^{\mathrm{he}}(a,\theta,\phi)=-\frac{I\,\mathrm{d}s^{\mathrm{he}}\eta\Delta_{gs}\cos\phi}{2ha}\sum_{n}\Lambda_{n}^{e}\frac{\partial P_{\nu}(\cos(\pi-\theta))}{\sin\nu\pi\partial\theta}, \tag{2.155}$$

$$E_{\theta}^{\mathrm{he}}(a,\theta,\phi)=-\frac{\mathrm{i}I\,\mathrm{d}s^{\mathrm{he}}\eta\cos\phi}{2ha}\left\{-\frac{\Delta_{gs}\Delta_{gr}}{ka}\sum_{n}\Lambda_{n}^{e}S_{n}^{-2}\frac{\partial^{2}P_{\nu}(\cos(\pi-\theta))}{\sin\nu\pi\partial\theta^{2}}\right.$$

$$\left.-\frac{1}{ka\sin\theta}\sum_{m}\Lambda_{m}^{h}S_{m}^{-2}\frac{\partial^{2}P_{\mu}(\cos(\pi-\theta))}{\sin\mu\pi\partial\theta}\right\}, \tag{2.156}$$

$$E_{\phi}^{\mathrm{he}}(a,\theta,\phi)=\frac{\mathrm{i}I\,\mathrm{d}s^{\mathrm{he}}\eta\sin\phi}{2ha}\left\{-\frac{\Delta_{gr}\Delta_{gs}}{ka\sin\theta}\sum_{n}\Lambda_{n}^{e}S_{n}^{-2}\frac{\partial P_{\nu}(\cos(\pi-\theta))}{\sin\nu\pi\partial\theta}\right.$$

$$\left.-\frac{1}{ka}\sum_{m}\Lambda_{m}^{h}S_{m}^{-2}\frac{\partial^{2}P_{\mu}(\cos(\pi-\theta))}{\sin\mu\pi\partial\theta^{2}}\right\}, \tag{2.157}$$

$$H_{r}^{\mathrm{he}}(a,\theta,\phi)=\frac{I\,\mathrm{d}s^{\mathrm{he}}\sin\phi}{2ha}\sum_{m}\Lambda_{n}^{h}\frac{\partial P_{\mu}(\cos(\pi-\theta))}{\sin\mu\pi\partial\theta}, \tag{2.158}$$

$$H_{\theta}^{\mathrm{he}}(a,\theta,\phi)=\frac{I\,\mathrm{d}s^{\mathrm{he}}\sin\phi}{2ha}\left\{-\mathrm{i}\frac{\Delta_{gs}}{ka\sin\theta}\sum_{n}\Lambda_{n}^{e}S_{n}^{-2}\frac{\partial P_{\nu}(\cos(\pi-\theta))}{\sin\phi\pi\partial\theta}\right.$$

$$\left.-\frac{\mathrm{i}}{ka\Delta_{gr}}\sum_{m}\Lambda_{m}^{h}S_{m}^{-2}\frac{\partial^{2}P_{\mu}(\cos(\pi-\theta))}{\sin\mu\pi\partial\theta^{2}}\right\}, \tag{2.159}$$

$$H_{\phi}^{\mathrm{he}}(a,\theta,\phi)=\frac{I\,\mathrm{d}s^{\mathrm{he}}\cos\phi}{2ha}\left\{-\frac{\mathrm{i}\Delta_{gs}}{ka}\sum_{n}\Lambda_{n}^{e}S_{n}^{-2}\frac{\partial^{2}P_{\mu}(\cos(\pi-\theta))}{\sin\upsilon\pi\partial\theta^{2}}\right.$$

$$\left.-\frac{\mathrm{i}}{ka\sin\theta\Delta_{gr}}\sum_{m}\Lambda_{m}^{h}S_{m}^{-2}\frac{\partial P_{\mu}(\cos(\pi-\theta))}{\sin\mu\pi\partial\theta}\right\}. \tag{2.160}$$

From the above six formulas for the field components, it is seen that field components consist of both TM and TE modes. It is well known that only a TM_0 wave can propagate while the rest of the waves are evanescent, which play roles in the far-field regions.

At large distance between the observation point and the dipole source, the components in the far-field regions are simplified as follows:

$$E_r^{\mathrm{he}}(a,\theta,\phi) = -\frac{I\,\mathrm{d}s^{\mathrm{he}}\eta\Delta_{gs}\cos\phi}{2ha}\Lambda_0^e\frac{\partial P_\nu(\cos(\pi-\theta))}{\sin\nu_0\pi\partial\theta}, \tag{2.161}$$

$$E_\theta^{\mathrm{he}}(a,\theta,\phi) = \frac{\mathrm{i}I\,\mathrm{d}s^{\mathrm{he}}\eta\Delta_{gs}}{2ha}\Delta_{gr}\cos\phi\frac{\Lambda_0^e}{ka}S_0^{-2}\frac{\partial^2 P_{\nu_0}(\cos(\pi-\theta))}{\sin\nu_0\pi\partial^2\theta}, \tag{2.162}$$

$$E_\phi^{\mathrm{he}}(a,\theta,\phi) = -\frac{\mathrm{i}I\,\mathrm{d}s^{\mathrm{he}}\eta}{2ha}\sin\phi\Delta_{gs}\Delta_{gr}\frac{\Lambda_0^e}{ka\sin\theta}S_0^{-2}\frac{\partial P_{\nu_0}(\cos(\pi-\theta))}{\sin\nu_0\pi\partial\theta}, \tag{2.163}$$

$$H_\theta^{\mathrm{he}}(a,\theta,\phi) = -\frac{\mathrm{i}I\,\mathrm{d}s^{\mathrm{he}}}{2ha}\Delta_{gs}\frac{\sin\phi}{ka\sin\theta}\Lambda_0^e S_0^{-2}\frac{\partial P_{\nu_0}(\cos(\pi-\theta))}{\sin\nu_0\pi\partial\theta}, \tag{2.164}$$

$$H_\phi^{\mathrm{he}}(a,\theta,\phi) = -\frac{\mathrm{i}I\,\mathrm{d}s^{\mathrm{he}}}{2ha}\Delta_{gs}\frac{\cos\phi}{ka}\Lambda_0^e S_0^{-2}\frac{\partial^2 P_{\nu_0}(\cos(\pi-\theta))}{\sin\nu_0\pi\partial^2\theta}, \tag{2.165}$$

where both Δ_{gs} and Δ_{gr} refer to the normalized surface impedances at the points for the transmitting antenna and the receiving antenna, respectively. It is seen that SLF/ELF field of an HED in the Earth–ionosphere waveguide or cavity is proportional to the surface impedance at the source point. In order to improve the radiation efficiency of the transmitting antenna, SLF/ELF antenna should be chosen to be located at the region where the Earth's surface has large surface impedance or low conductivity.

At large distance between the dipole source and the observation point, and where the observation point is not close to the antipole, for the range of $f > 50$ Hz, we have

$$\begin{aligned}\frac{P_\nu(\cos(\pi-\theta))}{\sin\nu\pi} &\approx -\sqrt{\frac{2}{\pi(\nu+0.5)\sin\theta}}\exp\left[\mathrm{i}(\nu+0.5)\theta+\mathrm{i}\frac{\pi}{4}\right]\\ &\approx -\sqrt{2}(\pi kaS_n\sin\theta)^{-1/2}\exp\left(\mathrm{i}kaS_n\theta+\mathrm{i}\frac{\pi}{4}\right).\end{aligned} \tag{2.166}$$

Then, it follows that

$$\frac{\partial P_\nu(\cos(\pi-\theta))}{\sin\nu\pi\partial\theta} \approx -\mathrm{i}\sqrt{\frac{2kaS_n}{\pi\sin\theta}}\exp\left(\mathrm{i}kaS_n\theta+\mathrm{i}\frac{\pi}{4}\right), \tag{2.167}$$

$$\frac{\partial^2 P_\nu(\cos(\pi-\theta))}{\sin\nu\pi\partial^2\theta} \approx \sqrt{\frac{2}{\pi\sin\theta}}(kaS_n)^{3/2}\exp\left(\mathrm{i}kaS_n\theta+\mathrm{i}\frac{\pi}{4}\right). \tag{2.168}$$

Thus, we obtain readily:

$$\begin{aligned}E_r^{\mathrm{he}}(a,\theta,\phi) = {}& \frac{\mathrm{i}I\,\mathrm{d}s^{\mathrm{he}}\eta\Delta_{gs}\cos\phi}{2ha}\sqrt{\frac{2}{\pi\sin\theta}}\\ &\times(kaS_0)^{\frac{1}{2}}\Lambda_0^e\exp\left(\mathrm{i}kaS_0\theta+\mathrm{i}\frac{\pi}{4}\right),\end{aligned} \tag{2.169}$$

$$E_{\theta}^{\mathrm{he}}(a,\theta,\phi)=\frac{\mathrm{i}I\,\mathrm{d}s^{\mathrm{he}}\eta\Delta_{gs}}{2ha}\Delta_{gr}\cos\phi\sqrt{\frac{2}{\pi\sin\theta}}\times(ka)^{\frac{1}{2}}S_0^{-\frac{1}{2}}\Lambda_0^e\exp\left(\mathrm{i}kaS_0\theta+\mathrm{i}\frac{\pi}{4}\right),\tag{2.170}$$

$$E_{\phi}^{\mathrm{he}}(a,\theta,\phi)=-\frac{I\,\mathrm{d}s^{\mathrm{he}}\eta}{2ha}\sin\phi\Delta_{gs}\Delta_{gr}\sqrt{\frac{2}{\pi\sin\theta}}\times(ka)^{-\frac{1}{2}}S_0^{-\frac{3}{2}}\Lambda_0^e\frac{\exp(\mathrm{i}kaS_0\theta+\mathrm{i}\frac{\pi}{4})}{ka\sin\theta},\tag{2.171}$$

$$H_{\theta}^{\mathrm{he}}(a,\theta,\phi)=-\frac{I\,\mathrm{d}s^{\mathrm{he}}}{2ha}\Delta_{gs}\frac{\sin\phi}{ka\sin\theta}\sqrt{\frac{2}{\pi\sin\theta}}\times(ka)^{-\frac{1}{2}}S_0^{-\frac{3}{2}}\Lambda_0^e\exp\left(\mathrm{i}kaS_0\theta+\mathrm{i}\frac{\pi}{4}\right),\tag{2.172}$$

$$H_{\phi}^{\mathrm{he}}(a,\theta,\phi)=-\frac{\mathrm{i}I\,\mathrm{d}s^{\mathrm{he}}}{2ha}\Delta_{gs}\sqrt{\frac{2}{\pi\sin\theta}}\times(ka)^{\frac{1}{2}}S_0^{-\frac{1}{2}}\Lambda_0^e\cos\phi\exp\left(\mathrm{i}kaS_0\theta+\mathrm{i}\frac{\pi}{4}\right).\tag{2.173}$$

At small distance between the dipole source and the observation point, namely, $\theta\ll 1$, we have

$$\frac{P_{\nu}(\cos(\pi-\theta))}{\sin\nu\pi}\approx-\mathrm{i}H_0^{(1)}\left[\left(\nu+\frac{1}{2}\right)\theta\right],\tag{2.174}$$

$$\frac{\partial P_{\nu}(\cos(\pi-\theta))}{\sin\nu\pi\partial\theta}\approx\mathrm{i}\left(\nu+\frac{1}{2}\right)H_1^{(1)}\left[\left(\nu+\frac{1}{2}\right)\theta\right],\tag{2.175}$$

$$\frac{\partial^2 P_{\nu}(\cos(\pi-\theta))}{\sin\nu\pi\partial^2\theta}\approx-\frac{\mathrm{i}(\nu+\frac{1}{2})H_1^{(1)}[(\nu+\frac{1}{2})\theta]}{\theta}.\tag{2.176}$$

Then, the formulas for the components in the near-field regions are rewritten in the following forms:

$$E_r^{\mathrm{he}}(a,\theta,\phi)=-\frac{I\,\mathrm{d}s^{\mathrm{he}}\eta\Delta_{gs}}{2ha}\cos\phi\cdot\left[\mathrm{i}ka\sum_n\Lambda_n^eS_nH_1^{(1)}(kaS_n\theta)\right],\tag{2.177}$$

$$E_{\theta}^{\mathrm{he}}(a,\theta,\phi)=-\frac{\mathrm{i}I\,\mathrm{d}s^{\mathrm{he}}\eta}{2ha}\cos\phi\cdot\left[\frac{\mathrm{i}\Delta_{gs}\Delta_{gr}}{\theta}\sum_n\Lambda_n^eS_n^{-1}H_1^{(1)}(kaS_n\theta)-\frac{\mathrm{i}}{\sin\theta}\sum_m\Lambda_m^hS_m^{-1}H_1^{(1)}(kaS_m\theta)\right],\tag{2.178}$$

$$E_{\phi}^{\mathrm{he}}(a,\theta,\phi)=\frac{\mathrm{i}I\,\mathrm{d}s^{\mathrm{he}}\eta}{2ha}\sin\phi\cdot\left[-\frac{\mathrm{i}\Delta_{gs}\Delta_{gr}}{\sin\theta}\sum_{n}\Lambda_{n}^{e}S_{n}^{-1}H_{1}^{(1)}(kaS_{n}\theta)\right.$$
$$\left.+\frac{\mathrm{i}}{\theta}\sum_{m}\Lambda_{m}^{h}S_{m}^{-1}H_{1}^{(1)}(kaS_{m}\theta)\right], \tag{2.179}$$

$$H_{r}^{\mathrm{he}}(a,\theta,\phi)=\frac{\mathrm{i}I\,\mathrm{d}s^{\mathrm{he}}}{2ha}\sin\phi\cdot\left[ka\sum_{m}\Lambda_{m}^{h}S_{m}H_{1}^{(1)}(kaS_{m}\theta)\right], \tag{2.180}$$

$$H_{\theta}^{\mathrm{he}}(a,\theta,\phi)=\frac{I\,\mathrm{d}s^{\mathrm{he}}}{2ha}\sin\phi\left[\frac{\Delta_{gs}}{\sin\theta}\sum_{n}\Lambda_{n}^{e}S_{n}^{-1}H_{1}^{(1)}(kaS_{n}\theta)\right.$$
$$\left.-\frac{1}{\Delta_{gr}}\sum_{m}\Lambda_{m}^{h}S_{m}^{-1}H_{1}^{(1)}(kaS_{m}\theta)\right], \tag{2.181}$$

$$H_{\phi}^{\mathrm{he}}(a,\theta,\phi)=\frac{I\,\mathrm{d}s^{\mathrm{he}}}{2ha}\cos\phi\left[-\frac{\Delta_{gs}}{\theta}\sum_{n}S_{n}^{-1}\Lambda_{n}^{e}H_{1}^{(1)}(kaS_{n}\theta)\right.$$
$$\left.+\frac{1}{\sin\theta\,\Delta_{gr}}\sum_{m}\Lambda_{m}^{h}S_{m}^{-1}H_{1}^{(1)}(haS_{m}\theta)\right]. \tag{2.182}$$

2.5 Effect of Phase Velocity and Attenuation Rate by Gradual Inhomogeneous Anisotropic Ionosphere in SLF/ELF Ranges

In the above sections, the region of interest is treated as ideal homogeneous isotropic spherical Earth–ionosphere cavity or waveguide. Under practical propagation conditions, the electron density and collision frequency in the ionosphere vary as the height, and the ionosphere is usually regarded as a gradient plasma. Because the wavelengths of SLF/ELF waves are very long, the radio waves can penetrate into the ionosphere deeply, even up to F_2-layer. Therefore, it is necessary to consider the effects on the attenuation and phase velocity by the ionospheric profile in SLF/ELF ranges. In practical computations on the attenuation rate and phase velocity, the ionosphere should be treated as a gradient layered plasma, while the effect by the geomagnetic field should also be considered. Obviously, the reflection characteristics of actual inhomogeneous anisotropic ionosphere can be equivalent to those of a reflection boundary at a certain reference height with an equivalent impedance matrix.

In SLF/ELF ranges, only the TM_0 wave can propagate in the Earth–ionosphere waveguide or cavity. Thus, it is only necessary to carry out the computations on the attenuation rate and the phase velocity for the TM_0 wave. With second-order spherical approximation, the calculation accuracy for the modal equation can be guaranteed. Therefore, the modal equation of SLF/ELF waves in the Earth–ionosphere

waveguide or cavity is obtained readily. It is

$$\begin{aligned}&\left[\left(1+R_h\mathrm{e}^{2\mathrm{i}kH}\right)-C'\Delta_{22}\left(1-R_h\mathrm{e}^{2\mathrm{i}kH}\right)\right]\\&\quad\times\left[C'\left(1-R_g\mathrm{e}^{2\mathrm{i}kH}\right)+\Delta_{11}\left(1+R_g\mathrm{e}^{2\mathrm{i}kH}\right)\right]\\&\quad+C'\Delta_{12}\Delta_{21}\left(1+R_g\mathrm{e}^{2\mathrm{i}kH}\right)\left(1-R_h\mathrm{e}^{2\mathrm{i}kH}\right)=0,\end{aligned}\tag{2.183}$$

where Δ_{ij} $(i,j=1,2)$ refer to the elements of the normalized surface impedance matrix of the ionosphere, which are satisfied to the following equation. We write

$$\begin{bmatrix}E_\theta\\E_\phi\end{bmatrix}=\eta\begin{bmatrix}\Delta_{11}\Delta_{12}\\\Delta_{21}\Delta_{22}\end{bmatrix}\begin{bmatrix}H_\theta\\H_\phi\end{bmatrix}.\tag{2.184}$$

Then, the modal equation (2.183) can be rewritten in the form

$$\begin{aligned}&\left(1-R_{g\parallel}R_\parallel\mathrm{e}^{2\mathrm{i}k_0H}\right)\left(1-R_h\ {}_\perp R_\perp\mathrm{e}^{2\mathrm{i}k_0H}\right)\\&\quad-{}_\parallel R_\perp\ {}_\perp R_\parallel R_hR_g\mathrm{e}^{4\mathrm{i}k_0H}=0,\end{aligned}\tag{2.185}$$

where

$$H=\int_0^h\left(C^2+\frac{2t}{a}S^2\right)^{1/2}\mathrm{d}t,\tag{2.186}$$

$$R_g=\frac{C-\Delta_g}{C-\Delta_g},\tag{2.187}$$

$$R_h=\frac{C-\Delta_g^{-1}}{C+\Delta_g^{-1}},\tag{2.188}$$

$$C'=\left(C^2+\frac{2h}{a}S^2\right)^{1/2}.\tag{2.189}$$

It is noted that the relations between the reflection coefficient matrix and the normalized surface impedance matrix are written as follows:

$${}_\parallel R_\parallel=\frac{(C'-\Delta_{11})(C'\Delta_{22}-1)+C'\Delta_{12}\Delta_{21}}{(C'+\Delta_{11})(C'\Delta_{22}-1)-C'\Delta_{12}\Delta_{21}},\tag{2.190}$$

$${}_\parallel R_\perp=\frac{-2C'\Delta_{21}}{(C'+\Delta_{11})(C'\Delta_{22}-1)-C'\Delta_{12}\Delta_{21}},\tag{2.191}$$

$${}_\perp R_\parallel=\frac{-2C'\Delta_{12}}{(C'+\Delta_{11})(C'\Delta_{22}-1)-C'\Delta_{12}\Delta_{21}},\tag{2.192}$$

$${}_\perp R_\perp=\frac{(C'+\Delta_{11})(1+C'\Delta_{22})-C'\Delta_{12}\Delta_{21}}{(C'+\Delta_{11})(C'\Delta_{22}-1)-C'\Delta_{12}\Delta_{21}}.\tag{2.193}$$

Next, the procedures for solving the modal equation are addressed as follows:

(1) First we assume that the Earth and the ionosphere are simplified as homogeneous isotropic media with sharp boundaries. From Eqs. (2.38) and (2.39), the roots (C_0, S_0) of the modal equation for TM_0 wave can be obtained readily. Then, we set the roots (C_0, S_0) as initial approximated values.
(2) With the root C_0, the incident angle cosine C' for the TM_0 wave can be obtained readily by Eq. (2.189).
(3) With the incident angle cosine C', and the profiles for both ionospheric electron density and collision frequency varying with the height, the equivalent surface impedance matrix of the ionosphere can be computed easily.
(4) Substituting the parameters of the ionospheric surface impedance matrix into the transcendental equation (2.183), the new incident angle cosine $C_i = C_0 + \triangle C$ can be obtained by using Newton's iteration method with the initial value C_0.
(5) The first-order approximated parameter C_i' for the corresponding ionospheric incident angle cosine can be solved by using Eq. (2.105) with the parameter C_i.
(6) Generally speaking, the ionospheric surface impedance matrix has little change to the incident angle in SLF/ELF ranges, so that the iteration computation repeating the procedures 3 to 5 for two or three times is enough to guarantee the accuracy.

With the roots of the modal equation, both the phase velocity and the attenuation rate of the TM_0 wave can be obtained readily:

$$\frac{c}{v_p} = \mathrm{Re}\, S, \tag{2.194}$$

$$\alpha = 8.6858k\, \mathrm{Im}\, S = 0.02895\omega\, \mathrm{Im}\, S\ (\mathrm{dB}/1000\ \mathrm{km}). \tag{2.195}$$

In SLF/ELF ranges, the ground surface impedance is much smaller than the ionospheric surface impedance. Evidently, the change of the ground conductivity has little effect on the phase velocity and attenuation rate of the TM_0 wave. In the practical computation, the ground is usually idealized to the sea surface.

In order to compare quantitatively the effects of the phase velocity and the attenuation rate by different ionosphere structure in SLF/ELF ranges, we choose the three ionospheric models to carry out the numerical calculations. The first ionospheric model is that of the ionosphere idealized as a homogeneous non-ideal plasma, for which the equivalent conductivity is $\sigma = 10^{-6}$ S/m. The second model is the reference structure of the lower ionosphere by the suggestions in the CCIR-895 report, which is characterized by

$$N(z) = 1.43 \times 10^7 \cdot \mathrm{e}^{-0.15H} \cdot \mathrm{e}^{(\beta-0.15)(z-H)}, \tag{2.196}$$

$$\nu(z) = 1.816 \times 10^{11} \cdot \mathrm{e}^{-0.15z}. \tag{2.197}$$

In the above formulas, N is the electron density in $1/\mathrm{cm}^3$, ν is the electron collision frequency in s^{-1}, z is the height of the observation point in km, and H is the

Table 2.1 The recommended values of H and β in mid-latitude regions

	Summer	Winter
Daytime	$\beta = 0.3$, $H = 70$	$\beta = 0.3$, $H = 72$
Nighttime	$\beta = 0.0077f + 0.31$, $H = 87$	$\beta = 0.0077f + 0.31$, $H = 87$

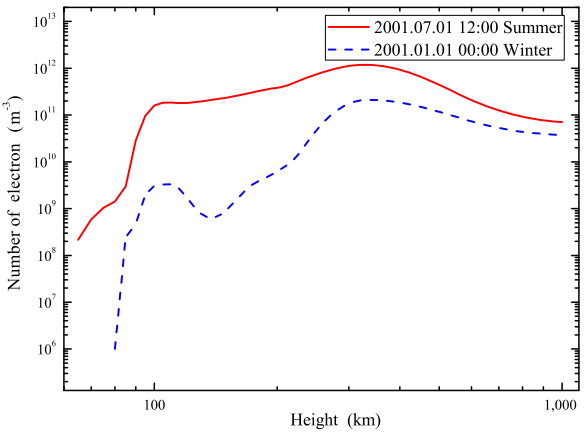

Fig. 2.7 For the international reference ionosphere model, the ionospheric electron density varying as the height in summer daytime and winter nighttime

ionospheric reference height in km. The recommended values of H in km and β in 1/km for mid-latitude regions are shown in Table 2.1. Here f is the operating frequency in kHz.

The third model is the international reference ionosphere model, in which the electron density profiles vary with the height in summer daytime and winter nighttime as shown in Fig. 2.7 (Rawer et al. 1978). The collision frequency varying with the height is taken as Eq. (2.197) for the exponential model.

For the above three ionosphere models, following the computational method and process addressed in this section, the modal equation for the SLF/ELF ranges is solved readily, and the characteristic parameters of each mode can be calculated easily. The attenuation rate on the sea surface versus the operating frequency for the fundamental mode (TM_0 mode or quasi-TEM mode) is computed for daytime and shown in Fig. 2.8. In Fig. 2.9, the corresponding calculated results in nighttime are given. The attenuation rates in nighttime on the sea surface versus the operating frequency for TM_1 and TE_1 modes are computed and shown in Figs. 2.10 and 2.11, respectively.

From the above computations, it is concluded as follows:

- In SLF/ELF ranges, the attenuation rate of the fundamental mode will increase as the operating frequency increasing. However, the attenuation rate is very small overall. Thus SLF/ELF waves can propagate to thousands kilometers or over ten thousand kilometers away from the transmitter, even for any place in the Earth–ionosphere waveguide or cavity.

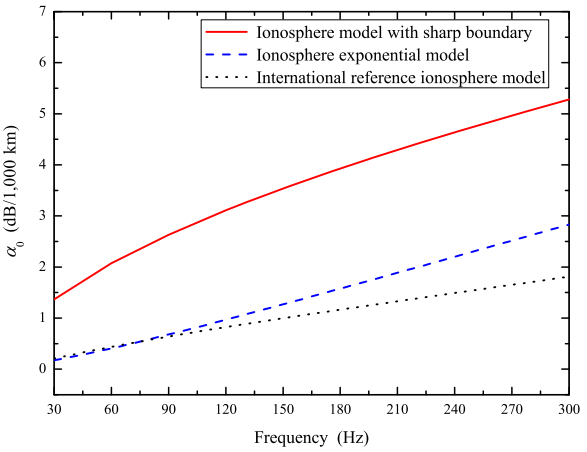

Fig. 2.8 The attenuation rate in daytime versus the operating frequency for the fundamental mode

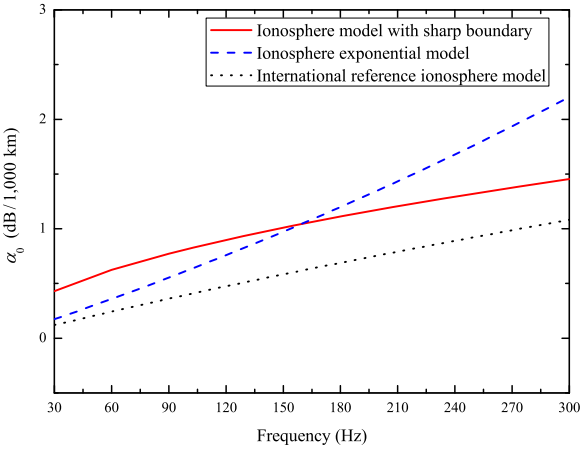

Fig. 2.9 The attenuation rate in nighttime versus the operating frequency for the fundamental mode

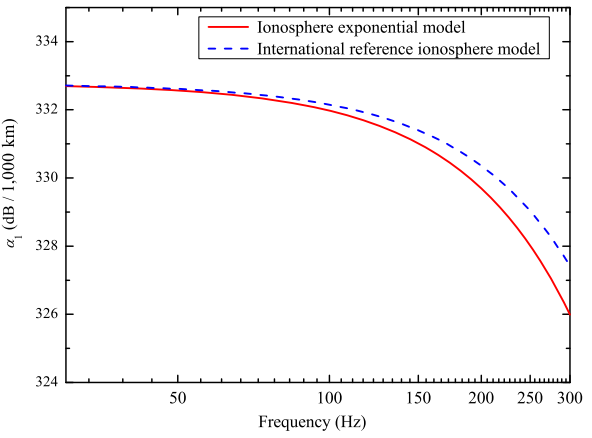

Fig. 2.10 The attenuation rate in nighttime versus the operating frequency for the TM_1 mode

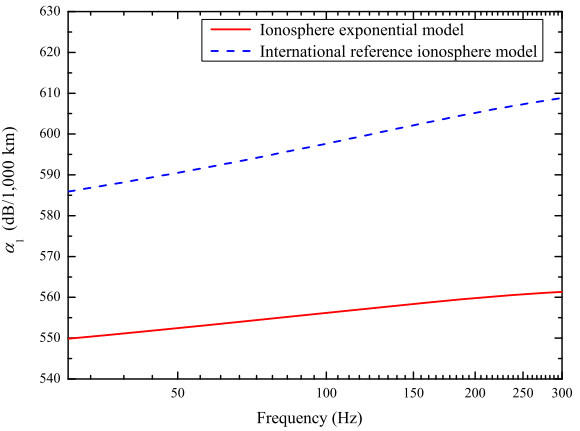

Fig. 2.11 The attenuation rate in nighttime versus the operating frequency for the TE_1 mode

- The attenuation rates for the high-order modes in SLF/ELF ranges are very large, generally several hundred dB/Mm. Thus, there only exists one propagating mode in SLF/ELF ranges.
- For the three different ionospheric models, although the parameters for each order modes are different from each other, the overall trends are consistent. In the case that the observer is located on or near the Earth's surface, it is acceptable to use a relatively simple model in engineering.
- From the computed results, it is seen that the propagation loss of SLF/ELF waves in daytime is larger than that in nighttime. It is resulted by the equivalent reflection height of the ionosphere in nighttime being higher than that in daytime.

The attenuation rates of the fundamental mode versus the ground conductivity are computed for the two different modes and shown in Fig. 2.12, respectively. It is seen that the attenuation rates decrease with the Earth's conductivity increasing, but the changing amplitudes are not large. This is resulted by the fact that the higher the ground conductivity is, the larger the reflections are, and the less the absorption loss of SLF/ELF waves are.

It is noted that the effect by the geomagnetic field is not considered in the computations in Figs. 2.8–2.12. Namely, the ionosphere is regarded as a one-dimensionally planar stratified isotropic plasma in the above computations. In lower frequency ranges, it is necessary to consider the effects by the geomagnetic field, and the ionosphere is regarded as an anisotropic plasma, which is characterized by using a 3×3 matrix. Especially in SLF/ELF ranges, the electromagnetic waves in the ionosphere will show significant anisotropic properties. In order to address the effects of the SLF/ELF wave propagation by the geomagnetic field, the computations for the relative phase velocity versus the propagation direction are carried out at $f = 75$ Hz and shown in Fig. 2.13. Similarly, with the same operating frequency,

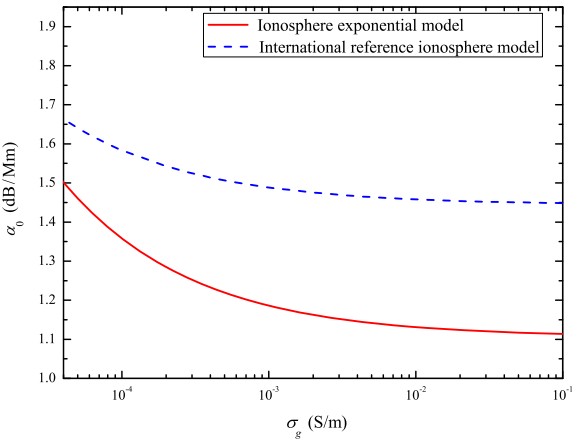

Fig. 2.12 The attenuation rate in nighttime versus the operating frequency for the TEM mode

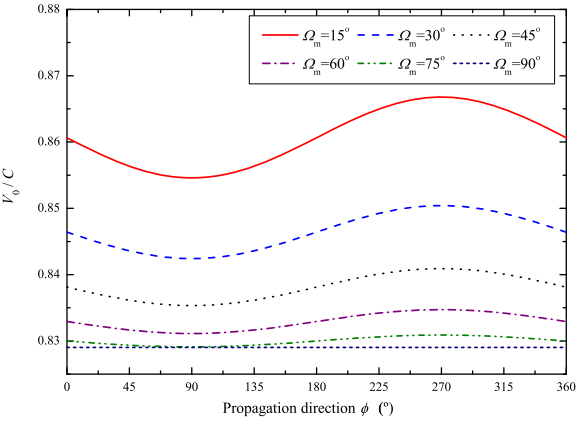

Fig. 2.13 The relative phase velocity versus the propagation direction at $f = 75$ Hz

the computations for the attenuation rates versus the propagation direction are also carried out and shown in Fig. 2.14. Magnitudes of the excitation factor for the fundamental mode versus the propagation direction are computed and shown in Fig. 2.15. In the computations in Figs. 2.13–2.15, the ionosphere model is taken as the second model as addressed in this section, the ionosphere reference height is $H = 70$ km, the ground conductivity is taken as $= 3$ S/m, and the geomagnetic field is taken as $B_0 = 0.5 \times 10^{-4}$ T.

From the above computations, we conclude as follows:

- For the attenuation rate and phase velocity of the fundamental mode, there exist directional actions. Obviously, the attenuation rate propagating eastward is smaller than that propagating westward, while the relative phase velocity propagating eastward is also smaller than that propagating westward.

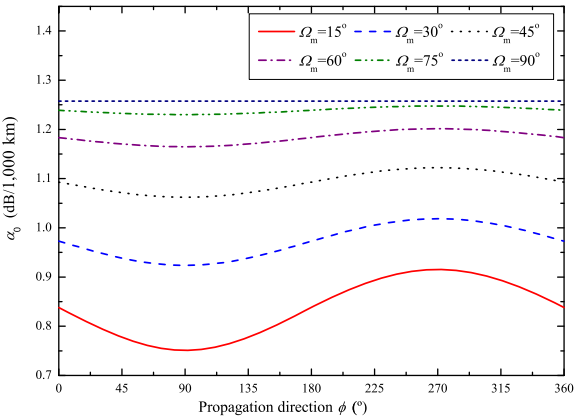

Fig. 2.14 The attenuation rates versus the propagation direction at $f = 75$ Hz

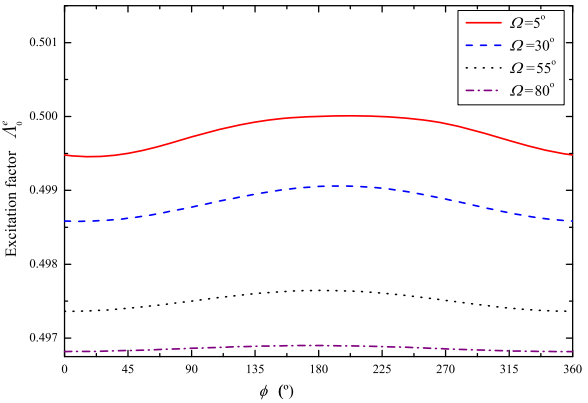

Fig. 2.15 The excitation factor for the fundamental mode versus the propagation direction at $f = 80$ Hz

- The attenuation rate and the phase velocity of the fundamental mode are affected by the geomagnetic inclination angle Ω. When the angle Ω is larger, the attenuation rate becomes larger, and the relative phase velocity is reduced correspondingly. Meanwhile, the effects of the attenuation rates and the phase velocity by the propagating direction are weakened.
- The attenuation rate and the phase velocity of the fundamental mode change slowly with the propagation direction and the geomagnetic inclination angle. Specifically, the effect of the attenuation rate is in the range of 0.1–0.4 dB/Mm, while the effect of the relative phase velocity is in the range of 1 %–3 %. Thus, the effects by the geomagnetic field are generally neglected.
- For the excitation factor of the fundamental mode, the effects by the geomagnetic field, which are usually neglected, was not significant with respect to that of the attenuation rate.

2.6 SLF/ELF Fields of Ground-Based Horizontal Transmitting Antenna

2.6.1 SLF Field in Far-Field Region

For practical ground-based SLF/ELF transmitting system, the transmitting antenna is generally an electrode antenna with both grounded ends and low-level frame. The antenna length is usually dozens of kilometers, even over 100 km. At large distance between the observation point and the transmitting antenna over 1,000 km, the transmitting antenna can be taken as an HED. In this case, along the whole of the propagating paths, both the ground and the ionosphere will be no longer homogeneous. Thus, the whole propagating path can be divided into several short uniform paths, of which each uniform path is a homogeneous waveguide. For each section of the Earth–ionosphere waveguide, the root S_0 can be obtained by solving the modal equation. The electromagnetic field in the Earth–ionosphere waveguide can be obtained by using the WKB solution. When the higher-order modes are neglected in the far-field region, the field components can be expressed in the following forms:

$$E_r = \frac{\mathrm{i}I\,\mathrm{d}l\eta\Delta_{gs}}{2ha}\sqrt{\frac{2ka}{\pi\sin\theta}}\cos\phi A_0^e(T)\left[S_0(T)S_0(R)\right]^{\frac{1}{4}} \times \exp\left[\mathrm{i}\int_0^\theta kaS_0\,\mathrm{d}\theta + \mathrm{i}\frac{\pi}{4}\right], \tag{2.198}$$

$$E_\theta = \frac{\mathrm{i}I\,\mathrm{d}l\eta}{2ha}\Delta_{gs}\Delta_{gr}\sqrt{\frac{2ka}{\pi\sin\theta}}\cos\phi A_e^0(T)\left[S_0(T)S_0(R)\right]^{-\frac{1}{4}} \times \exp\left[\mathrm{i}\int_0^\theta kaS_0\,\mathrm{d}\theta + \mathrm{i}\frac{\pi}{4}\right], \tag{2.199}$$

$$E_\phi = \frac{-I\,\mathrm{d}l\eta}{2ha}\sqrt{\frac{2}{\pi\sin\theta}}\frac{\Delta_{gs}\Delta_{gr}}{\sqrt{ka}\sin\theta}\sin\phi A_0^e(T)\left[S_0(T)S_0(R)\right]^{-\frac{3}{4}} \times \exp\left[\mathrm{i}\int_0^\theta kaS_0\,\mathrm{d}\theta + \mathrm{i}\frac{\pi}{4}\right], \tag{2.200}$$

$$H_\theta = \frac{-I\,\mathrm{d}l}{2ha}\sqrt{\frac{2}{\pi\sin\theta}}\frac{\Delta_{gs}\sin\phi}{\sqrt{ka}\sin\theta}A_0^e(T)\left[S_0(T)S_0(R)\right]^{-\frac{3}{4}} \times \exp\left[\mathrm{i}\int_0^\theta kaS_0\,\mathrm{d}\theta + \mathrm{i}\frac{\pi}{4}\right], \tag{2.201}$$

$$H_\phi = \frac{-\mathrm{i}I\,\mathrm{d}l}{2ha}\sqrt{\frac{2ka}{\pi\sin\theta}}\Delta_{gs}\cos\phi A_0^e(T)\left[S_0(T)S_0(R)\right]^{-\frac{1}{4}} \times \exp\left[\mathrm{i}\int_0^\theta kaS_0\,\mathrm{d}\theta + \mathrm{i}\frac{\pi}{4}\right], \tag{2.202}$$

where $S_0(T)$ and $S_0(R)$ represent the values of S_0 on the source point and the observation point, respectively. $\Lambda_0^e(T)$ represents the excitation factor on the source point, and both Δ_{gr} and Δ_{gs} represent the normalized surface impedance of the ground and that of the sea surface, respectively.

We assume that the local time of the transmitting point and that of the receiving point are in daytime and nighttime, respectively. Then, it is seen that the part of the ionosphere of the propagating path is in daytime, while the other part is in nighttime. The corresponding equivalent reflection height of the ionosphere in the circadian boundaries of the day-and-night transition period, there will be an obvious mutation, and there exists conversion between different modes. In the circadian boundaries of the unevenly transition period, the mode conversion coefficient is expressed in Eq. (2.203):

$$S_{nm} = \frac{\int_0^{H_{\min}} F_n^d(z) G_m^n(z)\,\mathrm{d}z}{\sqrt{\int_0^{H_1} [F_n^d(z)]^2\,\mathrm{d}z \cdot \int_0^{H_2} [G_n^d(z)]^2\,\mathrm{d}z}}, \tag{2.203}$$

where F_n^d and G_m^n represent the height-gain function for the nth-order mode of daytime and the mth-order mode of nighttime, respectively. H is the ionospheric reference height, $H_{\min} = \min(H_1, H_2)$.

With the mode conversion, in the circadian transitional period, the analytical formulas for SLF field components are obtained readily. We write

$$E_r = \frac{\mathrm{i}I\,\mathrm{d}l\eta\Delta_{gs}}{2\sqrt{h_d \times h_n}a}\sqrt{\frac{2ka}{\pi \sin\theta}}\cos\phi \cdot \left\{\sum_{n=1}^{N}\sum_{m=1}^{M} \Lambda_n^e(T) S_n^{\frac{1}{2}}(T) \times S_{nm} S_m^{\frac{1}{2}}(R) \exp\left[\mathrm{i}k\left(S_n^d R_d + S_m^n R_n\right) + \mathrm{i}\frac{\pi}{4}\right]\right\}, \tag{2.204}$$

$$E_\theta = \frac{\mathrm{i}I\,\mathrm{d}l\eta\Delta_{gs}\Delta_{gr}}{2\sqrt{h_d \times h_n}a}\sqrt{\frac{2ka}{\pi \sin\theta}}\cos\phi \cdot \left\{\sum_{n=1}^{N}\sum_{m=1}^{M} \Lambda_n^e(T) S_n^{\frac{1}{2}}(T) \times S_{nm} S_m^{\frac{1}{2}}(R) \exp\left[\mathrm{i}k\left(S_n^d R_d + S_m^n R_n\right) + \mathrm{i}\frac{\pi}{4}\right]\right\}, \tag{2.205}$$

$$E_\phi = \frac{-I\,\mathrm{d}l\eta}{2\sqrt{h_d \times h_n}a}\sqrt{\frac{2}{\pi \sin\theta}}\frac{\Delta_{gs}\Delta_{gr}}{\sqrt{ka}\sin\theta}\sin\phi \cdot \left\{\sum_{n=1}^{N}\sum_{m=1}^{M} \Lambda_n^e(T) S_n^{\frac{1}{2}}(T) \times S_{nm} S_m^{\frac{1}{2}}(R) \exp\left[\mathrm{i}k\left(S_n^d R_d + S_m^n R_n\right) + \mathrm{i}\frac{\pi}{4}\right]\right\}, \tag{2.206}$$

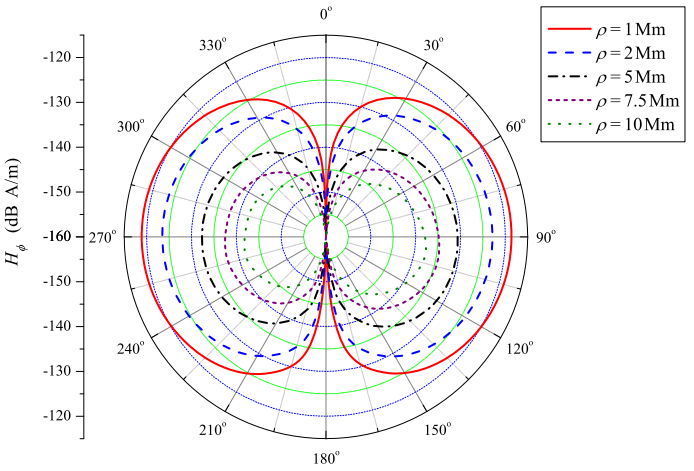

Fig. 2.16 The radiation pattern of the horizontal magnetic field components H_ϕ excited by an HED in East–West direction: $I = 350$ A, $\mathrm{d}l = 100$ km, $f = 80$ Hz, $\sigma_g(T) = 0.2 \times 10^{-3}$ S/m, and $\sigma_g(R) = 10^{-3}$

$$H_\theta = \frac{-I\,\mathrm{d}l}{2\sqrt{h_d \times h_n}a}\sqrt{\frac{2}{\pi \sin\theta}}\frac{\Delta_{gs}\sin\phi}{\sqrt{ka}\sin\theta} \cdot \left\{\sum_{n=1}^{N}\sum_{m=1}^{M} A_n^e(T) S_n^{\frac{1}{2}}(T) \times S_{nm} S_m^{\frac{1}{2}}(R) \exp\left[\mathrm{i}k\left(S_n^d R_d + S_m^n R_n\right) + \mathrm{i}\frac{\pi}{4}\right]\right\}, \tag{2.207}$$

$$H_\phi = \frac{-\mathrm{i}I\,\mathrm{d}l}{2\sqrt{h_d \times h_n}a}\sqrt{\frac{2ka}{\pi \sin\theta}}\Delta_{gs}\cos\phi \cdot \left\{\sum_{n=1}^{N}\sum_{m=1}^{M} A_n^e(T) S_n^{\frac{1}{2}}(T) \times S_{nm} S_m^{\frac{1}{2}}(R) \exp\left[\mathrm{i}k\left(S_n^d R_d + S_m^n R_n\right) + \mathrm{i}\frac{\pi}{4}\right]\right\}, \tag{2.208}$$

where h_d and h_n represent the ionospheric reference height of the daytime and that of the nighttime, respectively. R_d and R_n are the propagation distance of the daytime and that of the nighttime, respectively. N and M represent the order of the wave modes of the daytime and that of the nighttime, respectively.

Following the above method, when the ground conductivities and all parameters of the ionosphere in the regions of the whole propagating paths are given, the distribution of the electromagnetic field on the Earth's surface can be determined and computed readily.

The radiation pattern of the horizontal magnetic field components H_ϕ and H_ρ excited by a horizontal line antenna, which is placed in East–West direction, are shown in Figs. 2.16 and 2.17, respectively. In these computations, the antenna length is $\mathrm{d}l = 100$ km, the antenna current is assumed to be $I = 350$ A, the operating frequency is $f = 80$ Hz, and the ground conductivity of the transmitting point and

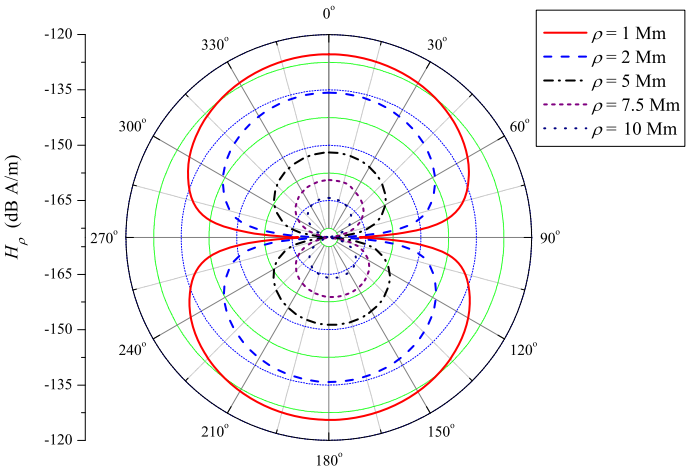

Fig. 2.17 The radiation pattern of the horizontal magnetic field components H_ρ excited by an HED in East–West direction: $I = 350$ A, d$l = 100$ km, $f = 80$ Hz, $\sigma_g(T) = 0.2 \times 10^{-3}$ S/m, and $\sigma_g(R) = 10^{-3}$

that of the observation point are taken as $\sigma_g(T) = 0.2 \times 10^{-3}$ S/m and $\sigma_g(R) = 10^{-3}$ S/m, respectively.

From Figs. 2.16 and 2.17, we conclude as follows:

- There is obviously directionality for the SLF field components excited by a horizontal line antenna. For the horizontal line antenna in the East–West direction, the main radiation direction of the component H_ϕ is in the East–West direction, while that of the component H_ρ is in the North–South direction.
- At approximately the same propagating distance, the magnitude of the component H_ϕ is much larger than that of the component H_ρ.
- The attenuation rate for the wave propagating eastward is smaller than that for the wave propagating westward, and considering the effects by the uneven ground conductivities, the field strength of the antenna east is larger than that of the west. Obviously, the radiation contour diagram is not completely symmetrical.

2.6.2 SLF Field in the Near-Field Region

In practice, the SLF/ELF transmitting antenna is fairly large in size. At small distances between the observation point and the transmitting antenna, especially the distance being comparable to the actual antenna length, it is unsuitable that the antenna is idealized as an HED. In this case, the transmitting antenna is usually divided into many small segments, of which each segment is regarded as an HED, and the total field can be understood as the superposition of the fields excited by all these HEDs. The radiation pattern of the horizontal magnetic field components

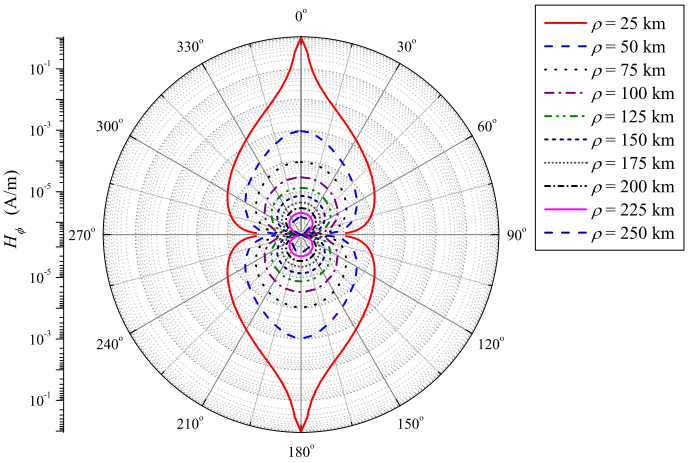

Fig. 2.18 The radiation pattern of the horizontal magnetic field components H_ϕ excited by an HED in South–North direction: $I = 62.5$ A, d$l = 80$ km, $f = 91$ Hz, $\sigma_g(T) = 0.2 \times 10^{-3}$ S/m, and $\sigma_g(R) = 10^{-3}$ S/m

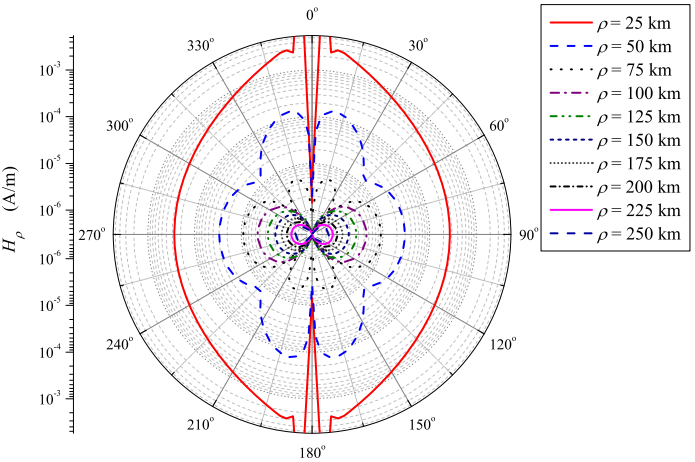

Fig. 2.19 The radiation pattern of the horizontal magnetic field components H_ρ excited by an HED in South–North direction: $I = 62.5$ A, d$l = 80$ km, $f = 91$ Hz, $\sigma_g(T) = 0.2 \times 10^{-3}$ S/m, and $\sigma_g(R) = 10^{-3}$ S/m

H_ϕ and H_ρ excited by a horizontal line antenna with its length 80 km in South–North direction are shown in Figs. 2.18 and 2.19, respectively. In these computations, we take $I = 62.5$ A, d$l = 80$ km, $f = 91$ Hz, $\sigma_g(T) = 0.2 \times 10^{-3}$ S/m, and $\sigma_g(R) = 10^{-3}$ S/m. From Figs. 2.16–2.19, it is seen that the radiation pattern in the near-field region is significantly different from that in the far-field region.

2.6.3 The Field in ELF Range and the Lower End of SLF Range

In the whole ELF range as well as the lower end of SLF range, the wavelength can be compared with, even exceeds, the Earth's circumference. At this time, for the eigenvalue ν of the zero-order TM wave, the condition of $\nu \gg 1$ is no longer satisfied. Thus the Legendre function of the first kind $P_\nu(\cos(\pi-\theta))$ should not be evaluated by using the traditional asymptotic formula in Eq. (2.29). In Sect. 2.2.4, the numerical integrated algorithm is proposed for evaluating the function $P_\nu(\cos(\pi-\theta))$. Then, the field in ELF range and the lower end of SLF range generated by an HED in the Earth–ionosphere cavity can be computed by using the new proposed algorithm (Peng et al. 2013).

In the case of an HED, the analytical formulas for the electromagnetic field in the Earth–ionosphere cavity have been obtained in Sect. 2.4. In these formulas, all components are expressed in terms of $\frac{\partial P_\nu(\cos(\pi-\theta))}{\partial\theta}$ and $\frac{\partial^2 P_\nu(\cos(\pi-\theta))}{\partial\theta^2}$. In order to evaluate accurately these components, it is necessary to give the new algorithm for evaluating the functions $\frac{\partial P_\nu(\cos(\pi-\theta))}{\partial\theta}$ and $\frac{\partial^2 P_\nu(\cos(\pi-\theta))}{\partial\theta^2}$.

As mentioned in Sect. 2.4, we denote

$$\phi(\nu,\theta)=\frac{1}{\sin\nu\pi}P_\nu\big(\cos(\pi-\theta)\big), \tag{2.209}$$

and

$$\begin{aligned}\frac{\partial}{\partial\theta}\phi(\nu,\theta)&=\frac{1}{\sin\nu\pi}\frac{\partial}{\partial\theta}P_\nu\big(\cos(\pi-\theta)\big)\\&=\frac{\nu}{\sin\theta}\big[\phi(\nu,\theta)\cos\theta-\phi(\nu-1,\theta)\big].\end{aligned} \tag{2.210}$$

From the above equations, we obtain readily:

$$\begin{aligned}\frac{\partial^2}{\partial\theta^2}\phi(\nu,\theta)=\frac{\nu}{\sin^2\theta}\big[&\big(\nu\cos^2\theta-1\big)\phi(\nu,\theta)\cos\theta-2(\nu-1)\cos\theta\phi(\nu-1,\theta)\\&+(\nu-1)\phi(\nu-2,\theta)\big].\end{aligned} \tag{2.211}$$

With the substitutions of Eqs. (2.209)–(2.211) into Eqs. (2.155)–(2.160), we readily derive the following. We write

$$E_r=-\frac{I\,\mathrm{d}l\eta\Delta_g}{2ha}\cos\phi\cdot\sum_{n=0}^{\infty}\Lambda_n^e\frac{\partial P_{\nu_n}(\cos(\pi-\theta))}{\sin(\nu_n\pi)\partial\theta}, \tag{2.212}$$

$$\begin{aligned}E_\theta=\frac{\mathrm{i}I\,\mathrm{d}l\eta}{2ha}\cos\phi\cdot\Bigg\{&\frac{\Delta_g^2}{ka}\sum_{n=0}^{\infty}\frac{\Lambda_n^e}{S_n^2}\frac{\partial^2 P_{\nu_n}(\cos(\pi-\theta))}{\sin(\nu_n\pi)\partial\theta^2}\\&+\frac{1}{ka\sin\theta}\sum_{m=1}^{\infty}\frac{\Lambda_m^h}{S_m^2}\frac{\partial P_{\mu_m}(\cos(\pi-\theta))}{\sin(\mu_m\pi)\partial\theta}\Bigg\},\end{aligned} \tag{2.213}$$

$$E_\phi = -\frac{\mathrm{i}I\,\mathrm{d}l\eta}{2ha}\sin\phi\cdot\left\{\frac{\Delta_g^2}{ka\sin\theta}\sum_{n=0}^{\infty}\frac{\Lambda_n^e}{S_n^2}\frac{\partial P_{\nu_n}(\cos(\pi-\theta))}{\sin(\nu_n\pi)\partial\theta}\right.$$
$$\left.+\frac{1}{ka}\sum_{m=1}^{\infty}\frac{\Lambda_m^h}{S_m^2}\frac{\partial^2 P_{\mu_m}(\cos(\pi-\theta))}{\sin(\mu_m\pi)\partial\theta^2}\right\}, \tag{2.214}$$

$$H_r = \frac{I\,\mathrm{d}l}{2ha}\sin\phi\cdot\sum_{m=1}^{\infty}\Lambda_m^h\frac{\partial P_{\mu_m}(\cos(\pi-\theta))}{\sin(\mu_m\pi)\partial\theta}, \tag{2.215}$$

$$H_\theta = -\frac{\mathrm{i}I\,\mathrm{d}l}{2ha}\sin\phi\cdot\left\{\frac{\Delta_g}{ka\sin\theta}\sum_{n=0}^{\infty}\frac{\Lambda_n^e}{S_n^2}\frac{\partial P_{\nu_n}(\cos(\pi-\theta))}{\sin(\nu_n\pi)\partial\theta}\right.$$
$$\left.+\frac{1}{ka\Delta_g}\sum_{m=1}^{\infty}\frac{\Lambda_m^h}{S_m^2}\frac{\partial^2 P_{\mu_m}(\cos(\pi-\theta))}{\sin(\mu_m\pi)\partial\theta^2}\right\}, \tag{2.216}$$

$$H_\phi = -\frac{\mathrm{i}I\,\mathrm{d}l}{2ha}\cos\phi\cdot\left\{\frac{\Delta_g}{ka}\sum_{n=0}^{\infty}\frac{\Lambda_n^e}{S_n^2}\frac{\partial^2 P_{\nu_n}(\cos(\pi-\theta))}{\sin(\nu_n\pi)\partial\theta^2}\right.$$
$$\left.+\frac{1}{ka\Delta_g\sin\theta}\sum_{m=1}^{\infty}\frac{\Lambda_m^h}{S_m^2}\frac{\partial P_{\mu_m}(\cos(\pi-\theta))}{\sin(\mu_m\pi)\partial\theta}\right\}. \tag{2.217}$$

In these equations, the functions $\frac{\partial P_\mu(\cos(\pi-\theta))}{\partial\theta}$ and $\frac{\partial^2 P_\mu(\cos(\pi-\theta))}{\partial\theta^2}$ can be computed by using Eqs. (2.77), (2.210), and (2.211).

We assume that the unit HED is placed at $\theta = 0°$ in the direction of $\phi_T = 0°$ and the operating frequency is taken as $f = 10$ Hz. As shown in Figs. 2.20 and 2.21, with the orientation of the observation point $\phi = 0°$, the magnitudes of the components E_θ and H_ϕ are computed by using the numerical integrated algorithm proposed in this chapter and the traditional method (Bannister 1984), respectively. With the orientation of the observation point $\phi = 90°$, similar computations are carried out for the components E_ϕ and H_θ and also plotted in Figs. 2.20 and 2.21, respectively.

From Figs. 2.20 and 2.21, it is seen that the computed results by using the two methods are significantly different from each other in ELF range and the lower end of SLF range (below 50 Hz). The traditional method by Bannister (1984) is based on the assumption of $\nu \gg 0$, so that it is only suitable for the SLF range. Correspondingly, the results by using the traditional method is uncorrect for the range below 50 Hz. In ELF range and the lower end of SLF range, the distributions of the electromagnetic field on the ground can be evaluated accurately by using the numerical integrated method proposed in this chapter.

We assume that the current moment of the transmitting antenna, which is placed horizontally in the $\hat{x}$ direction, is taken as 1 A·m, the ionospheric reference height is 70 km, and the conductivities of the ground and the ionosphere are assumed as $\sigma_g = 10^{-3}$ S/m and $\sigma_i = 10^{-5}$ S/m, respectively. The contour diagram of the tan-

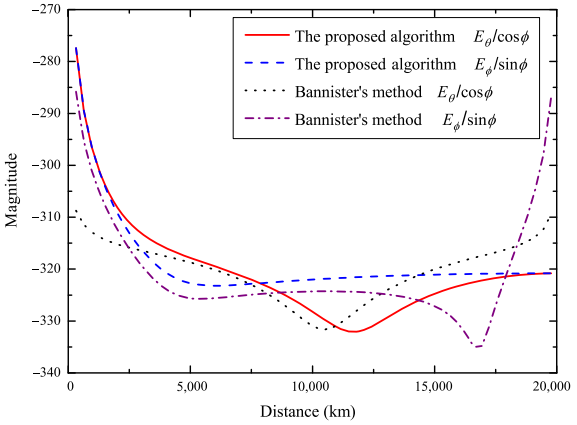

Fig. 2.20 The magnitudes of the components E_θ in dB·V/m at $\phi = 90°$ and E_ϕ in dB·V/m at $\phi = 0°$ versus the propagation distance: $f = 10$ Hz, $\phi_T = 0°$

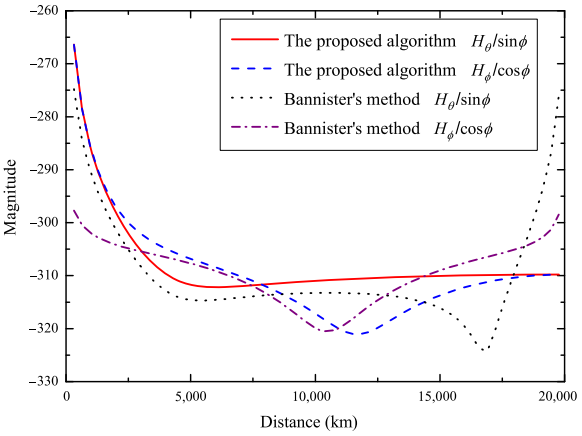

Fig. 2.21 The magnitudes of the components H_ϕ in dB·A/m at $\phi = 0°$ and H_ϕ in dB·A/m at $\phi = 90°$ versus the propagation distance: $f = 10$ Hz, $\phi_T = 0°$

gential electric field and that of the tangential magnetic field at $f = 1$ Hz are shown in Figs. 2.22 and 2.23, respectively. It is noted that all numbers in the above contour diagrams indicate the field strength in dB. For the electric field, 1 V/m is corresponded to 0 dB. For the magnetic field, 1 A/m is corresponded to 0 dB.

At the operating frequency below 2 Hz, the wavelength is much larger than the Earth's circumference, and the space between the Earth's surface and the lower boundary of the ionosphere is actually a concentric spherical shell. Obviously, the eigenvalue ν is smaller than 1. With Eq. (836.7) in the mathematics handbook by Gradshteyn and Ryzhik (1980), we write

$$\left.\frac{\partial P_\nu(\cos(\pi-\theta))}{\partial \nu}\right|_{\nu=0} = 2\ln\sin\left(\frac{\theta}{2}\right). \tag{2.218}$$

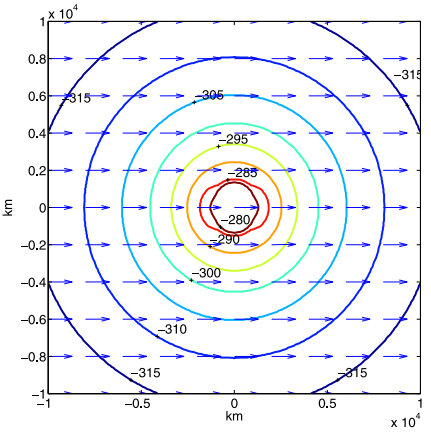

Fig. 2.22 The contour diagram of the tangential electric field at $f = 1$ Hz

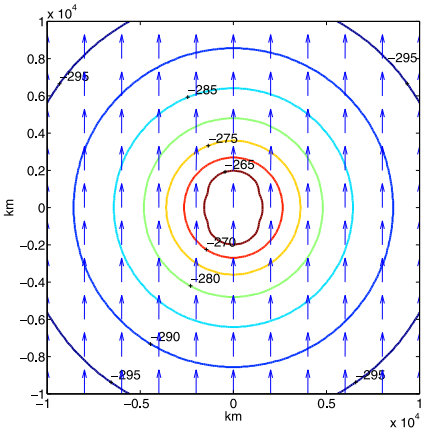

Fig. 2.23 The contour diagram of the tangential magnetic field at $f = 1$ Hz

When $\nu \ll 1$, we have

$$P_\nu\big(\cos(\pi-\theta)\big) = 1 + 2\nu \ln \sin\left(\frac{\theta}{2}\right) + O\big(\nu^2\big). \tag{2.219}$$

If a first-order approximation is taken, we obtain readily:

$$\frac{1}{\sin\theta}\frac{\partial P_\nu(\cos(\pi-\theta))}{\partial\theta} \approx \frac{\partial^2 P_\nu(\cos(\pi-\theta))}{\partial\theta^2}. \tag{2.220}$$

Thus, at the operating frequency below 2 Hz, in the far-field region, the higher modes attenuate rapidly, and the electromagnetic field excited by an HED essentially satisfies the following conditions:

$$\frac{E_\theta}{\cos\phi} = -\frac{E_\phi}{\sin\phi}; \qquad \frac{H_\theta}{\sin\phi} = \frac{H_\phi}{\cos\phi}. \tag{2.221}$$

Then, the horizontal field components are expressed in the following forms:

$$\mathbf{E_t} = E_\theta(\hat{\theta}\cos\phi - \hat{\phi}\sin\phi) = E_\theta \hat{x}, \tag{2.222}$$

$$\mathbf{H_t} = H_\theta(\hat{\theta}\sin\phi + \hat{\phi}\cos\phi) = H_\theta \hat{y}. \tag{2.223}$$

Evidently, the horizontal electric field is essentially in the $\hat{x}$ direction, while the horizontal magnetic field is essentially in the $\hat{y}$ direction. Furthermore, it is seen that both the horizontal electric field and the horizontal magnetic field will not change with the azimuth angle ϕ.

From Figs. 2.22 and 2.23, we conclude as follows:

- At the operating frequency below 2 Hz, except for the multimode region, which the transmitting antenna is surrounded nearby, all curves in the contour diagrams are approximately concentric circles. Namely, at the same distance away from the transmitting antenna, the tangential components of the electromagnetic field are essentially equal.
- At the operating frequency below 2 Hz, the direction of the tangential electric field component is essentially the same as that of the current moment, while the direction of the tangential magnetic field component is essentially perpendicular to that of the current moment.

When the operating frequency increases, the condition of $\nu \ll 1$ is no longer satisfied. For example, at $f = 10$ Hz, the parameter ν is comparable to 1, $\nu \sim 1$. The direction of the tangential electric field component is not completely the same as that of the current moment, while the direction of the tangential magnetic field component is not completely perpendicular to that of the current moment.

References

Bannister PR (1984) ELF propagation update. IEEE J Ocean Eng 9(3):179–188

Bannister PR, Wolkoff EA, Katan JR, Williams FJ (1973) Far-field, extremely-low-frequency propagation measurements. Radio Sci 8(7):623–631

Barrick DE (1999) Exact ULF/ELF dipole field strengths in the Earth–ionosphere cavity over the Schumann resonance region: idealized boundaries. Radio Sci 34(1):209–227

Bouwkamp CJ, Casimir HBG (1954) On multipole expansions in the theory of electromagnetic radiation. Physica 20:539–554

Budden KG (1961) Radio waves in the ionosphere. Cambridge University Press, Cambridge

Carroll KJ, Ferraro AJ (1990) Computer simulation of ELF injection in the Earth–ionosphere waveguide. Radio Sci 25(6):1363–1367

Cummer SA (2000) Modeling electromagnetic propagation in the Earth–ionosphere waveguide. IEEE Trans Antennas Propag 48(9):468–474

Felsen LB, Marcuvitz N (1973) Radiation and scattering of waves, Englewood Cliffs. Prentice Hall, New York

Fraser-Smith AC, Bannister PR (1998) Reception of ELF signals at antipodal distance. Radio Sci 33(1):83–88

Galejs J (1964) Terrestrial extremely-low-frequency propagation. In: Bleil DF (ed) Natural electromagnetic phenomena below 30 kc/s. Plenum, New York, pp 205–258

Galejs J (1968) ELF and VLF fields of a horizontal electric dipole. IEEE Trans Antennas Propag 16(6):689–700
Galejs J (1970) ELF and VLF propagation for models of a perturbed ionosphere. Radio Sci 5(7):1041–1044
Galejs J (1972a) Terrestrial propagation of long electromagnetic waves. Pergamon, New York
Galejs J (1972b) Stable solutions of ionospheric fields in the propagation of ELF and VLF waves. Radio Sci 7(6):549–561
Gradshteyn IS, Ryzhik IM (1980) Table of integrals, series, and products. Academic Press, New York
Kirillov VV, Pronin AE (2007) Normal waves of the anisotropic Earth–ionosphere waveguide in the VLF-ULF range. Int J Geomagn Aeron 7:GI2006. doi:10.1029/2005GI000126G
Li GZ (2012) Researches on mechanism of SLF and ELF wave propagation in an anisotropic Earth-ionosphere cavity. MS thesis, Zhejiang University, Hangzhou, China. (In Chinese)
Nickolaenko AP, Hayakawa M (2002) Resonances in the Earth–ionosphere cavity. Kluwer Academic, Dordrecht
Pan WY (2004) LF VLF ELF wave propagation. UESTC Press, Chengdu. (In Chinese)
Peng HY, Tao W, Pan WY, Guo LX (2012) Numerical integral method for ELF fields excited by vertical electric dipole in asymmetric Earth–ionosphere cavity. Chin J Radio Sci 22(2):333–338. (In Chinese)
Peng HY, Wu SH, Pan WY, Guo LX (2013) ELF fields excited by horizontal electric dipole in asymmetric Earth–ionosphere cavity. Submitted to Chin J Radio Sci. (In Chinese)
Rawer K, Bilitza D, Ramakrishnan S (1978) Goals and status of the international reference ionosphere. Rev Geophys 16:177–181
Rybachek ST, Ponomariev MJ (2007) Efficiency of the Earth–ionosphere waveguide excitation by ELF sources located in an anisotropic ionosphere. Int J Geomagn Aeron 7:GI1005. doi:10.1029/2005GI000123
Suchumann WO (1952a) On the radiation free selfoscillations of a conducting sphere, which is surrounded by an air layer and an ionosphere shell. Z Naturforsch 72:149–154. (In German)
Suchumann WO (1952b) On the damping of electromagnetic selfoscillations of the system Earth–air–ionosphere. Z Naturforsch 72:250–252. (In German)
Tripathi VK, Chang CL, Papadopoulos K (1982) Excitation of the Earth–ionosphere waveguide by an ELF source in the ionosphere. Radio Sci 17(5):1321–1326
Wait JR (1957) The mode theory of VLF ionospheric propagation for finite ground conductivity. Proc IRE 45(6):760–767
Wait JR (1960) Terrestrial propagation of very-low-frequency radio waves, a theoretical investigation. J Res Natl Bur Stand 64D:153–204
Wait JR (1970) Electromagnetic waves in stratified media, 2nd edn. Pergamon, New York
Wait JR (1992) Reflection of VLF radio waves at a junction in the Earth-ionosphere waveguide. IEEE Trans Electromagn Compat 34:4–8
Wait JR, Spies KP (1965) Influence of finite ground conductivity on the propagation of VLF radio waves. Radio Sci 3:787–791
Wang YX, Peng Q, Pan WY, Zhang HQ, Zhang ZW (2005) The fields excited by SLF/ELF horizontal electric dipole in Earth–ionosphere cavity. Chin J Radio Sci 22(5). (In Chinese)
Wang YX, Fan WS, Pan WY, Zhang HQ (2008) Spherical harmonic series solution of fields excited by vertical electric dipole in Earth–ionosphere cavity. Front Electr Electron Eng China 3(1):61–69

http://www.springer.com/978-3-642-39049-4

Propagation of SLF/ELF Electromagnetic Waves

Pan, W.-Y.; Li, K.

2014, X, 265 p. 132 illus., Hardcover
ISBN: 978-3-642-39049-4